# Preparation and magnetic property of $MN_y$ (M=Mn, Co, Ni)

Mitsuharu Tabuchi

Osaka University
February, 1994

# Preparation and magnetic property of $MN_y$ (M=Mn, Co, Ni)

Mitsuharu Tabuchi

Osaka University
February, 1994

**Contents**

## Chapter 1 General introduction

*1. Historical background of this study*

"Nitride" is the compound consist of nitrogen and metal elements (M). Metal nitrides are classified by bonding nature into three categories, i.e., ionic nitride, covalent nitride and interstitial nitride. The constituent elements of ionic nitrides are alkaline and alkaline earth metals. The chemical formula of most ionic nitrides are given by $M_3N$ or $M_3N_2$ and their chemical compositions are close to be stoichiometric. In ionic nitride, the valence state of nitrogen is only minus three as $N^{3-}$. The ionic nature of M–N bonding reflects their characteristic properties such as high melting point in nitrogen atmosphere ($Ca_3N_2$ (1173K), $Mg_3N_2$ (1573K)), ionic conductivity and easy oxidation in air.

Covalent nitrides refer to the compounds containing later metals than copper in the periodic table. Most of these nitrides possess the stoichiometric composition as predicted from the valence of constituent elements, as well as ionic nitrides. The crystal structures of AlN, BN and GaN are wurtzite–type structure with $M_4N$ tetrahedron. Such the structural feature in AlN, BN and GaN suggests the covalent nature of metal–nitrogen bonding. The electronic properties of covalent nitrides are characterized to be semiconductor or insulator. Covalent nitrides are stable in air compared with ionic nitrides and have high melting point or high decomposition temperature (AlN (2473K), $Si_3N_4$ (2173K), etc.).

Transition metal nitrides ($MN_y$) are so–called interstitial nitrides. Most of $MN_y$ have crystal structures such as NaCl type (TiN, VN), anti–NiAs type ($Fe_{2-3}N$, $Cr_2N$) anti–perovskite type ($Fe_4N$) structures and so on, in which M atoms form the nearly closest packed structure such as hcp or fcc and N atoms occupy partially the octahedral interstitial sites of M lattice as shown in Fig. 1. $MN_y$ can possess the variety of crystal phases with the large nonstoichiometry compared to other nitrides. Various crystalline phases of 3d transition metal nitrides $MN_y$ have been reported [1] and are shown in Table 1. The

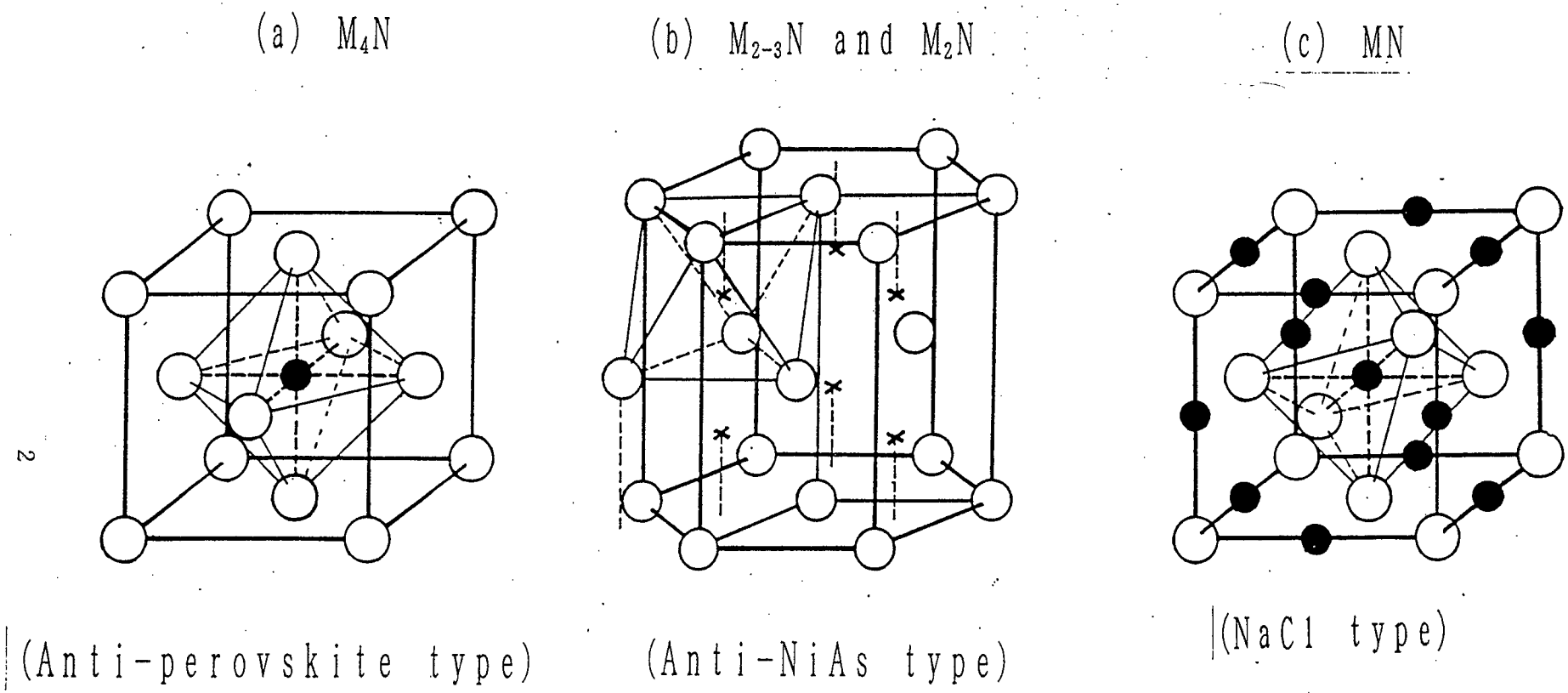


Fig. 1. Representative 3d transition metal nitrides $M_4N$ (a), $M_{2-3}N$, $M_2N$ (b) and MN (c). Open and closed circles denote 3d metal (M) and nitrogen (N), respectively. $M_6N$ octahedron are also shown in this figure. Octahedral interstitial sites are indicated in (b) by crosses.

representative crystal structure of $MN_y$ are classified into three categories, $M_4N$ (anti-Perovskite type structure), $M_{2-3}N$ (anti-NiAs type structure) and MN (NaCl type structure), as shown in Table 1. CoN [2] and FeN [2] possess zincblende type structure with $M_4N$ tetrahedron and differ from other nitrides such as TiN and VN with NaCl-type structure. Covalent nature of M-N bonding in $MN_y$ is presumed by the crystal structure of CoN and FeN. $MN_y$ exhibits diverse properties such as high melting point (e.g., TiN (3223K), ZrN (2973K)), brittleness, electric conductivity, superconductivity (NbN, TiN, MoN), ferromagnetism ($Fe_4N$, $Fe_{16}N_2$) and antiferromagnetism (CrN). These properties result from the coexistence of M-M bonding and M-N bonding in $MN_y$. In particular, 3d metal nitrides ($MN_y$) have the diversity of magnetic properties. Table 2 depicts the magnetic properties of $MN_y$ ($0 \leq y \leq 1$) [4-18]. The magnetism of most of 3d metal nitrides but for $CoN_y$ and $NiN_y$ are consistent with the magnetism of their mother metals as shown in Table 2.

$Cr_2N_{0.88}$ differ from Cr and CrN in the magnetism [4]. CrN exhibit the structural change at Néel temperature. The low temperature phase of CrN has an orthorhombic lattice with a deformed NaCl-type structure [19]. Antiferromagnetic structure of $Mn_3N_2$ was determined previously [6]. However, magnetic transition temperature ($T_{mag}$) of $Mn_3N_2$ and the magnetism of $Mn_6N_5$ is still unresolved.

The investigation of magnetic property of 3d metal nitrides has been focused mainly on the iron nitrides. Most of $FeN_y$ exhibits ferromagnetism analogous to $\alpha$-Fe (bcc) but the magnetism of $FeN_y$ in which Fe atoms take hcp or fcc lattice differs from antiferromagnetism of $\gamma$-Fe (fcc) and $\varepsilon$-Fe (hcp). The difference in the magnetism between $Fe_4N$ and $\gamma$-Fe was explained by magnetovolume effect, i.e., the lattice expansion accompanied by inclusion of N atoms caused the increase in magnetic moment per a metal atom ($\mu_M$) and Curie temperature ($T_c$) of $Fe_4N$ [20]. The magnetovolume effect has been also observed on $Y_2Fe_{17}N_y$ and $Y_2Fe_{17}C_y$ as shown in Fig 2 [21]. It has been reported

Table. 1 Crystal structure of 3d transition metal nitrides. The compounds designated in parentheses are only obtained by non-thermalequilibrium reaction processes.

| Ti | V | Cr | Mn | Fe | Co | Ni |
|---|---|---|---|---|---|---|
| | | | | $(Fe_{16}N_2)$ | | |
| | | | $Mn_4N$ | $Fe_4N$ | $(Co_4N)$ | $(Ni_4N)$ |
| $Ti_2N$ | $V_2N$ | $Cr_{2-3}N$ | $Mn_{2-3}N$ | $Fe_{2-3}N$ | $Co_3N$ | $Ni_3N$ |
| | | | | $Fe_2N$ | $Co_2N$ | $Ni_2N$ |
| | | | $Mn_3N_2$ | | | |
| TiN | VN | CrN | $Mn_6N_5$ | (FeN) | (CoN) | |

Table 2 Crystal structure and magnetic properties of $MN_y$ ($0 \leqq y \leqq 1$)[4].

| Compounds | Structure | Magnetism | $T_{mag}$/K | $\chi \times 10^6$/cm$^3$g$^{-1}$ | $\mu_M/\mu_B$ | $\mu_{eff}/\mu_B$ | Ref. |
|---|---|---|---|---|---|---|---|
| TiN | NaCl | PP | - | 1.0 | - | ICW | |
| Ti | hcp | PP | - | 3.2 | - | ICW | |
| VN | NaCl | PP | - | 2.0 | - | ICW | |
| $V_2N_{0.88}$ | $\varepsilon$-$Fe_{2-3}N$ | PP | - | 3.7 | - | ICW | |
| V | bcc | PP | - | 4.5 | - | ICW | |
| CrN | NaCl | AF | 283 | 3.98 | 2.4 (77K) | ICW | |
| $Cr_2N_{0.88}$ | $\varepsilon$-$Fe_{2-3}N$ | PP | - | 5.25 | - | ICW | |
| Cr | bcc | AF | 311 | 3.17 | 0.4 | ICW | |
| $Mn_6N_5$ | Mn: fct-fcc<br>N : ambiguous | - | - | - | - | - | [5] |
| $Mn_3N_2$ | Mn: fct<br>N : ordered | AF | - | 9.2 | 4.3,<br>3.4 (11K) | - | [6] |
| $Mn_2N$ | $\zeta$-$Fe_2N$(ortho) | AF | 301 | 15 | 1.6 | ICW | [7] |
| $Mn_4N$ | $Fe_4N$ | FI | 738 | - | 3.85<br>0.9 (77K) | ICW | [8] |
| $\gamma$-Mn | fct-fcc | AF | 480 | 8.5 | 2.4 | ICW | |
| $\alpha$-Mn | $\alpha$-Mn | AF | 95 | 8.9 | 1.9, 1.7,<br>0.6, 0.2. | ICW | |
| $FeN_{0.9}$ | Zinkblende | P | - | 15 | - | 1.7 | [3] |
| $Fe_2N$ | $\zeta$-$Fe_2N$(ortho) | F | 4 | 2.9 | 0.13 | 3.0 | [9] |
| $Fe_2N_{0.78}$ | $\varepsilon$-$Fe_{2-3}N$ | F | 398 | - | 1.9, 0.7 | D | [7, 10] |
| $Fe_4N$ | Perovskite | F | 761 | D | 3.0, 2.0 | D | [11] |
| $Fe_{16}N_2$ | Fe: bct<br>N : ordered | F | 813 | D | 1.36, 2.56,<br>3.86. | D | [12] |
| $\varepsilon$-Fe | hcp | AF | 100 | - | 0.1 | ICW | |
| $\gamma$-Fe | fcc | AF | 115 | - | 0.6 | ICW | |
| $\alpha$-Fe | bcc | F | 1043 | - | 2.2 | 3.20 | |
| CoN | Zinkblende<br>or NaCl | - | - | - | - | - | [2, 13] |
| $Co_2N$ | Anti-$CaCl_2$ | - | - | - | - | - | [14] |
| $Co_3N_{1.55}$ | $\varepsilon$-$Fe_{2-3}N$ | AF | 11 | 23 | - | 3 | [15] |
| $Co_4N$ | $Fe_4N$ | F | D | - | - | - | [16] |
| Co | hcp-fcc | F | 1388 | - | 1.7 | 3.15 | |
| $Ni_2N$ | Ni:bct<br>N: ordered | P | - | - | - | 0.14 | [17] |
| $Ni_3N_{1.16}$ | $\varepsilon$-$Fe_{2-3}N$ | P | - | - | 0.13 | - | [9] |
| $Ni_4N$ | $Fe_4N$ | - | - | - | - | - | [18] |
| Ni | fcc | F | 631 | - | 0.6 | 1.61 | |

$T_{mag}$; Magnetic transition temperature (K), $\chi$; Magnetic susceptibilities (cm$^3$/g) at 300K, $\mu_M$; Magnetic moment per a metal atom ($\mu_B$), $\mu_{eff}$; Effective magnetic moment per a metal atom.

P; Paramagnetism, PP; Pauli paramagnetism, AF; Antiferromagnetism, FI; ferrimagnetism, D; Decomposition at high temperature, ICW; Independence of Curie-Weiss law.

$T_{mag}$ of $Fe_{16}N_2$ were estimated by temperature dependence of magnetization below 673K.

Plural values of $\mu_M$ for $Mn_3N_2$, $Mn_4N$, $Fe_2N_{0.78}$, $Fe_4N$ and $Fe_{16}N_2$ are attributed to the presence of different metal sites in their structures.

that the insertion of small atoms such as H, C and N, into the $R_2Fe_{17}$ compounds (R=Y and rare earths) produce the volume expansion which increases the magnetic interaction between iron atoms and elevates Curie temperature of the compounds [21]. The increase in magnetic moment of Fe–N martensite with increasing nitrogen content has been explained by the use of the magnetovolume effect [22]. Values of $T_c$ and $\mu_{Fe}$ of $FeN_y$ with $y \leq 0.5$ have been found to decrease with increasing $y$ [4], as shown in Fig. 3. Mekata *et al.* [23] concluded that the N atoms suppressed magnetic ordering in consequence of the reduction of their magnetic moments. However, it has been found recently that the magnetic properties of $FeN_y$ with $y>0.5$ deviate from those tendency in the composition range of $y \leq 0.5$ [3].

Recently, Kim and Takahashi reported first that $Fe_{16}N_2$ exhibited a giant magnetic moment ($\mu_{Fe}=2.9\mu_B$) [24]. Since this finding, much interest have been paid on $Fe_{16}N_2$. The crystal structure of $Fe_{16}N_2$ is shown in Fig. 4 [25], and $Fe_{16}N_2$ have the three magnetic moments (1.3, 2.5 and $3.8\mu_B$) corresponding to the different Fe sites [26] in analogy with $Fe_4N$. The spin polarized band calculations for $Fe_{16}N_2$, $Fe_4N$ and $Fe_3N$ have been carried out [27].

While a little investigation has been reported on Co and Ni nitrides so far. The magnetic properties of $CoN_y$ have been rarely studied except those of $Co_3N$ [15] and $Co_4N$ [16]. The chemical composition of $Co_3N$ [15] was reported to be $Co_3N_{1.55}$ and deviates from that of previous data [28]. The lattice parameter of $Co_4N$ [16] was quite small, compared to that of $Co_4N_{1.0}$ [1] and is close to that of fcc–Co. The magnitude of the magnetization for $Ni_3N_{1.16}$ has been reported to be compatible with paramagnetism {9], but the detailed magnetic property has not been reported so far.

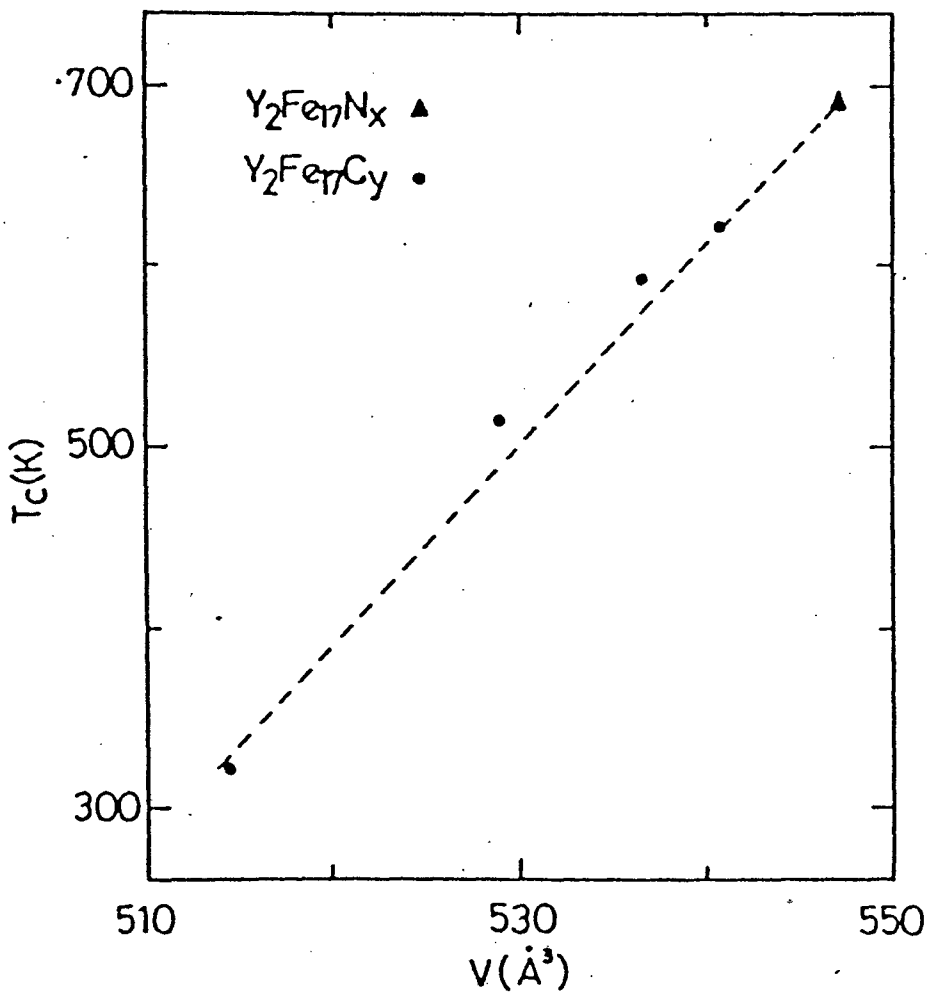


Fig. 2. Volume ($V$) dependence of Curie temperature ($T_c$) of $Y_2Fe_{17}N_x$ (▲) and $Y_2Fe_{17}C_y$ (●) [21]. The broken line represents the volume dependence of $Y_2Fe_{17}$.

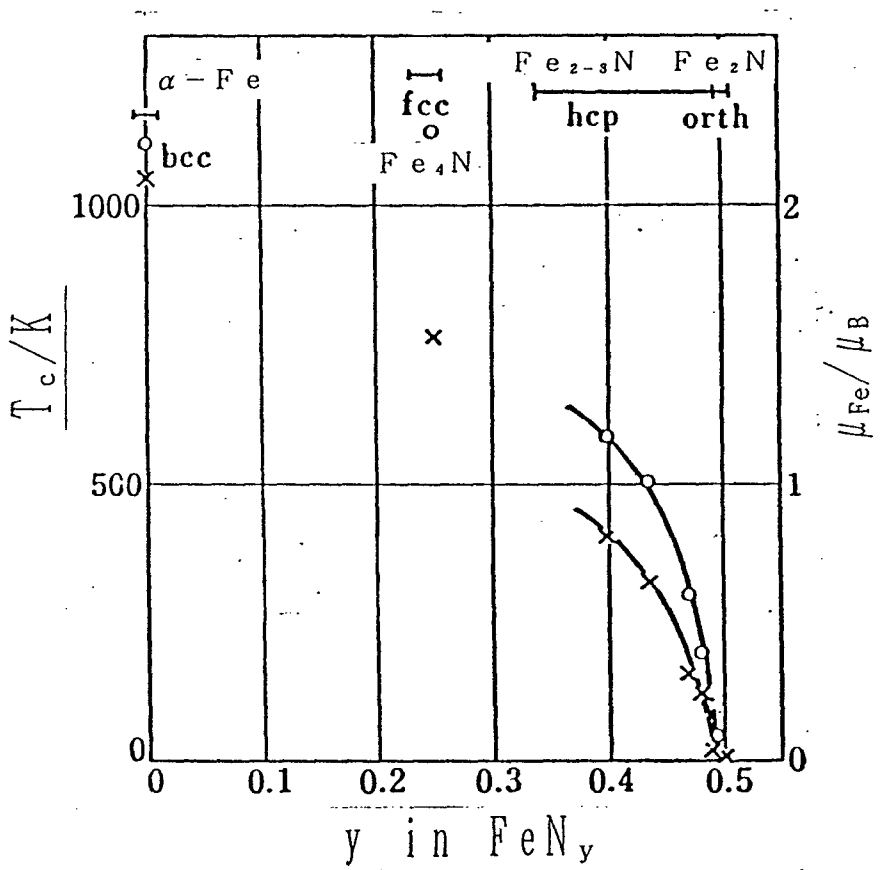


Fig. 3. Plots of the magnetic moments ($\mu_{Fe}$: O) and Curie temperature ($T_c$: ×) against the nitrogen contents of $FeN_y$ ($y \leq 0.5$) [4].

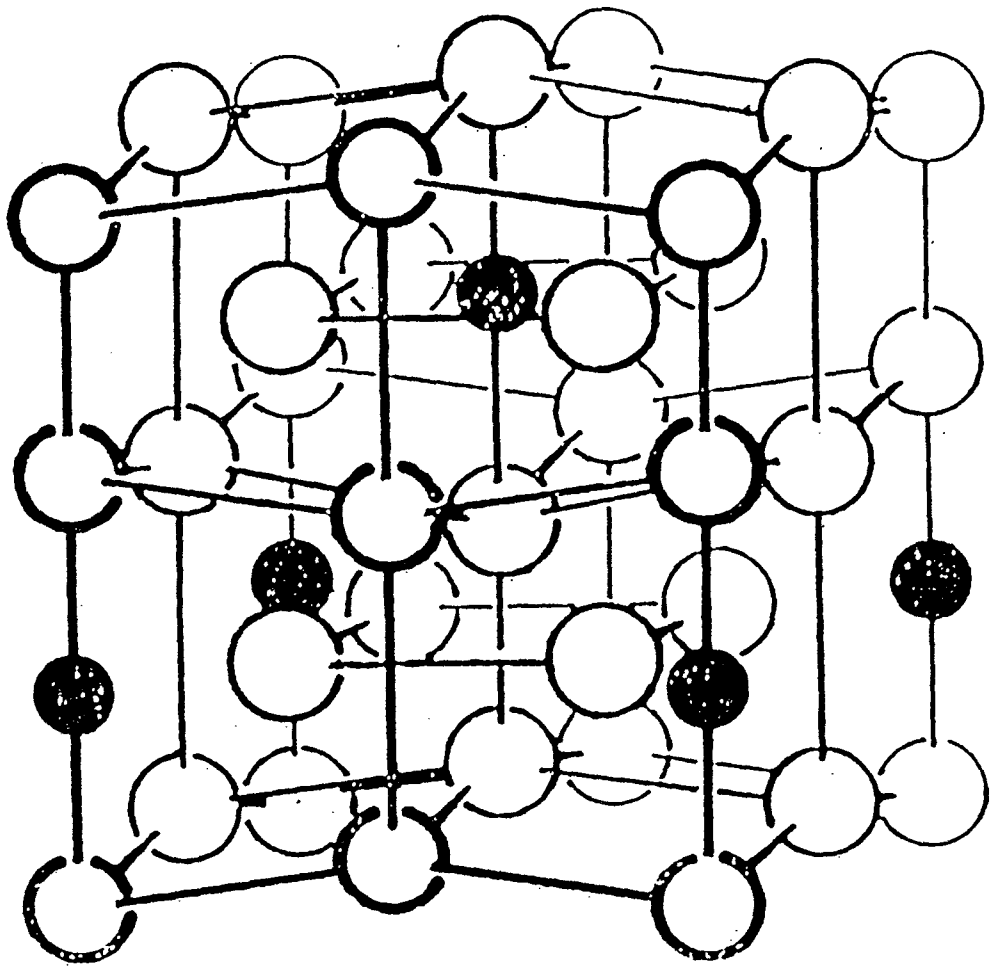

Fig. 4. Crystal structure of $Fe_{16}N_2$ [25]. Open and closed circles denotes Fe and N atoms, respectively.

*2. Purpose of this study*

Although numerous investigations in connection with the magnetic properties of 3d metal nitrides have been carried out so far, as described above, there remains several problems about the effect of nitrogen content on the magnetism of $MN_y$. N atoms in $MN_y$ have been said to suppress magnetic ordering in consequence of the reduction of their magnetic moments [23]. This concept can explain the decrease in the magnetic moment and magnetic transition temperature with increasing nitrogen content in $Fe_{2-3}N$ [23] (See Fig. 3.). However, the magnetic moment and magnetic transition temperature of $Fe_4N$ and $Fe_2N_{0.78}$ is larger than γ–Fe and ε–Fe, respectively, as shown in Table 2, can not be explained by this concept. This tendency has been well explained by the use of another concept, "magnetovolume effect". The effect of the nitrogen content on the magnetic properties of $MN_y$ has been interpreted coordinately. That is, some idea besides two concepts is required to understand the effect of nitrogen content on the magnetic properties of $MN_y$.

In this work, it is purposed that the effect of nitrogen content on the magnetic properties of $MN_y$ are understood comprehensively. In order to achieve this purpose, the following problems were elucidated systematically, (1) the determination of the factors which govern magnetic transition temperature, (2) the relation between the magnetic moment per a metal atom and N–coordination number and (3) the effect of the number of valence electrons per a metal atom on the magnetic properties.

In order to resolve these problems, the factors governed the magnetic transition temperature were first examined in $MnN_y$, because of the presence of various equilibrium phases over the wide range between 0 and 1 as compared to $CrN_y$, $FeN_y$, $CoN_y$ and $NiN_y$. The determination of $T_{mag}$ for $Mn_3N_2$ and $Mn_6N_5$ was carried out through measurements of temperature dependence of magnetic susceptibility, because the magnetic properties of $Mn_6N_5$ and $Mn_3N_2$ have not been clarified in detail. These results is described in chapter

2. The idea obtained by the examination of the factors affected the magnetic transition temperature of $MnN_y$, i.e., the relation between the magnetic transition temperature and the magnetic moment, is extended to other nitrides in chapter 3. The effect of number of valence electrons per a metal atom on the magnetic properties is investigated in chapter 4 by the use of $M_{2-3}N$ and $M_2N$ which exist over the many kinds of 3d metals. Temperature dependence of magnetic susceptibility for $Co_3N$, $Co_2N$ and $Ni_3N$ were also studied because of the lack of their magnetic property. Furthermore, $MnN_y$ films with various nitrogen content prepared by reactive vapor deposition method and the effect of ordering of nitrogen atoms on the electrical property are examined through temperature dependence of electrical resistivity of $MnN_y$ film (chapter 5). Finally, in chapter 6 is given the general discussion which based on the information of chapter 2, 3, 4 and 5.

*References*


1 R. Juza, *Adv. Inorg. Chem. Radiochem., 9* (1966) 81.

2 T. B. Joyner and F. H. Verhoek, *J, Am. Chem. Soc. 83* (1961) 1070.

3 M. Takahashi, H. Fujii, H. Nakagawa, S. Nasu and F. Kanamaru, *Proc. 6th International Conference on Ferrites,* The Japan Society of Powder and Powder Metallurgy, Tokyo and Kyoto, 1992, p. 508.

4 S. Chikazumi, K. Oota, K. Adachi, N. Tsuda and Y. Ishikawa (eds.), "*Jiseitai Handbook*", (Asakura-shoten) (1975).

5 N. Ōtsuka, Y. Hanawa and S. Nagakura, *Phys. Status Solidi A, 43* (1977) K127.

6 G. Kreiner and H. Jacobs, *J. Alloys Comp., 183* (1992) 345.

7 M. Mekata, J. Haruna and H. Takaki, *J. Phys. Soc. Jpn., 25* (1968) 234.

8 W. J. Takei, R. R. Heikes and G. Shirane, *Phys. Rev., 125* (1962) 1893.

9 J. B. Goodenough, A. Wold and R. J. Arnott, *J. Appl. Phys., 31* (1960) 342S.

10 K. H. Eickel and W. Pitsch, *Phys. Status Solidi, 39* (1970) 121.

11 B. C. Frazer, *Phys. Rev. 112* (1958) 751.

12 Y. Sugita, K. Mitsuoka and M. Komuro, *Nippon Oyo Jiki Gakkaishi, 15* (1991) 667.

13 O. Schmitz-Dumont, *Angew. Chem., 67* (1955) 231.

14 J. Clarke and K. H. Jack, *Chem. Ind. (London), 1951* (1951) 1004.

15 K. H. Mader, F. Thieme and A. Knappwost, *Z. Anorg. Allg. Chem. 366* (1969) 274.

16 K. Oda, T. Yoshio and K. Oda, *J. Mater. Sci., 22* (1987) 2729.

17 K. Ohta, Master Thesis of Osaka University (1992).

18 G. J. W. R. Dorman and M. Sikkens, *Thin Solid Films, 105* (1983) 251.

19 L. M. Corliss, N. Elliot and J. M. Hastings, *Phys. Rev. 117* (1960) 929.

20 A. Sakuma, *Nippon Oyo Jiki Gakkaishi, 17* (1993) 741.

21 L. Kong, L Cao and B. Shen, *J. Alloys. Comp., 191* (1993) 301.

22 K. Mitsuoka, H. Miyajima, H. Ino and S. Chikazumi, *J. Phys. Soc. Jpn., 53* (1984) 2381.

23 M. Mekata, H Yoshimura and H Takaki, *J. Phys. Soc. Jpn., 33* (1972) 62.

24 T. K. Kim and M. Takahashi, *J. Appl. Phys. Lett., 20* (1972) 492.

25 K. H. Jack, *Proc. Roy. Soc. (London), A208* (1951) 216.

26 K. Nakajima, S Okamoto M. Tanaka and H. Sekizawa, *Nippon Oyo Jiki Gakkaishi, 15* (1991) 703.

27 A. Sakuma, *J. Magn. Magn. Mater., 102* (1991) 127.

28 R. Juza and W Satze, *Z. Anorg. Chem., 253* (1945) 95.

## Chapter 2 Relation between magnetic transition temperature and magnetic moment for manganese nitrides $MnN_y$ (0<y<1)

### 1. *Introduction*

The magnetic properties of transition metal nitrides $MN_y$ are similar to those of their mother metals [1]. In particular, some of iron nitrides $FeN_y$ exhibit ferromagnetism in analogy with the magnetism of α–Fe. The magnetic properties of iron nitrides $FeN_y$, such as $Fe_4N$ [2], $Fe_{2-3}N$ [1] and $Fe_2N$ [1] have been well studied so far. Curie temperatures $T_c$ for $FeN_y$ ($y \leqq 0.5$) show a tendency that $T_c$ decrease with increasing $y$ [1, 3]. However, it has been found recently that one of phases of $FeN_y$ with $y>0.5$ indicates a deviation from the tendency in the composition range of $y \leqq 0.5$ [4]. The study on magnetic properties of $FeN_y$ ($y>0.5$) has been rarely investigated because $FeN_y$ with $y>0.5$ are formed only by applying non–thermal equilibrium reaction processes. In the case of chromium nitrides $CrN_y$, only $Cr_2N$ and CrN exist, respectively, as the phases on the Cr–N phase diagram and as regards cobalt nitrides $CoN_y$ and nickel nitrides $NiN_y$, only $Co_3N$, $Co_2N$ and $Ni_3N$ are stable phases in the Co–N and the Ni–N system. Consequently, discussions on the relation between the magnetic properties of metal nitrides and their nitrogen content, $y$ have been restricted within the range of $y$ less than 0.5.

On the other hand, the various crystal phases of $MnN_y$ with a variety of nitrogen content, such as $Mn_4N$, $Mn_{2-3}N$, $Mn_3N_2$ and $Mn_6N_5$ were reported on the Mn–N phase diagram [5]. The magnetic properties of $Mn_4N$ [6, 7] and $Mn_{2-3}N$ [1, 8] which have, respectively, the similar crystal structures as those of $Fe_4N$ and $Fe_{2-3}N$ were clarified previously. The antiferromagnetic structure of $Mn_3N_2$ below 291K was analyzed by unpolarized neutron diffraction measurements at 11 and 291K, and also by magnetic susceptibility measurement between 3.5K and room temperature [9], but magnetic transformation temperature of $Mn_3N_2$ was not determined. The magnetic property of

$Mn_6N_5$ was still remains unresolved. In this work, the magnetic properties of both $Mn_3N_2$ and $Mn_6N_5$ were clarified by magnetic susceptibility measurements from 100K to 958K, and then the magnetic transition temperature $T_{mag}$ of $MnN_y$ with $y$ ranging from 0 to 1 was discussed in connection with the shortest Mn–Mn distance and the magnetic moment per a Mn atom.

## 2. *Experimental*

$Mn_6N_5$ were prepared by heating α–Mn powder (99.9% in purity, Furuuchi Chemical Co.) at 873K for 3h in $NH_3$ gas flow, followed by annealing at 673K for 20h in the same atmosphere. $Mn_3N_2$ was obtained by heating α–Mn at 873K for 3h in $NH_3$ gas flow, followed by annealing in $H_2$ flowing at 873K for 1.5h. MnO, existed as a second phase in $Mn_6N_5$ and $Mn_3N_2$ was removed by washing with successive HCl aqueous solution, distilled water and ethanol. The concentration of HCl aq. solution used was 1.0 $moldm^{-3}$ and 0.1 $moldm^{-3}$ for $Mn_6N_5$ and $Mn_3N_2$, respectively.

The identification of products was carried out using a X–ray diffractmeter (CuKα radiation, Rotaflex/RINT, Rigaku Co). The lattice parameters of products were obtained from X–ray diffraction (XRD) measurement using silicon as an internal standard. The nitrogen and oxygen contents in products were determined by means of the apparatus for nitrogen and oxygen analysis (EMGA–2800, Horiba Co.).

The magnetic susceptibility of a sample was measured at 10.5kOe by a Faraday balance (MB–3, Shimazu Co.) in He atmosphere between 100 and 300K and in $N_2$ atmosphere between 300 and 958K, respectively. Mn Tutton's salt was used as a standard substance of magnetic susceptibility. The temperature was calibrated by magnetic transition temperatures of MnO (117.8K [10]), Ni (631.0K [10]) and α–$Fe_2O_3$ (953K [10]) used as standard materials. As trace amounts of spontaneous magnetization $\sigma_s$ from ferromagnetic impurity was observed, the external magnetic field dependence of the

magnetization σ of samples was measured at 80K, 300K, and in the vicinities of 740K and of 950K, respectively. The values of saturation magnetization $\sigma_s$ of the ferromagnetic impurity was evaluated from the value of σ extrapolated to zero magnetic field, $H$=0 in the σ–$H$ curve between 1.8 and 12.5kOe at each temperature.

Thermal gravimetry and differential thermal analyses, TG–DTA measurements for $Mn_6N_5$ and $Mn_3N_2$ were accomplished by using the instrument for thermal analysis (TG81110, Rigaku Co.) between 300 and 973K under $N_2$ gas flow and Ar gas flow, respectively.

## *3. Results and discussion*

### *3.1 Structure, composition and magnetic susceptibilities of $Mn_6N_5$ and $Mn_3N_2$*

Powder XRD patterns of $Mn_6N_5$ and $Mn_3N_2$ are shown in Fig. 1 (a) and (b), respectively. All diffraction lines of $Mn_6N_5$ could be indexed with a face centered tetragonal (fct) cell and those of $Mn_3N_2$ was indexed with three fold fct cell along the c–axis direction as reported previously [11], showing that ordering of nitrogen atoms in the fct Mn lattice took place in $Mn_3N_2$. The chemical composition of both samples was determined to be $Mn_6N_{5.35}$ and $Mn_3N_{1.93}$ by nitrogen and oxygen analysis. These values agreed, respectively, with $Mn_6N_{5.32}$ and $Mn_3N_{1.91}$ evaluated from the relationship between lattice parameter and composition of $MnN_y$ [12].

The DTA measurements of both $Mn_6N_5$ and $Mn_3N_2$ indicated that they took place the phase transition at 660–663K and 913–923K, respectively. Otsuka *et al* [13] found that $Mn_6N_5$ films transformed from fct to fcc at 683±20K by the electron diffraction measurement, and Jacobs and Stübe [11] observed the reversible phase transition of $Mn_3N_2$ at 903–928K by means of DTA measurement. The phase transition temperatures observed in this work agreed with these previous results. $Mn_3N_2$ possesses the fct structure of Mn atoms with the ordering of nitrogen atoms. Therefore, it could be presumed that crystal

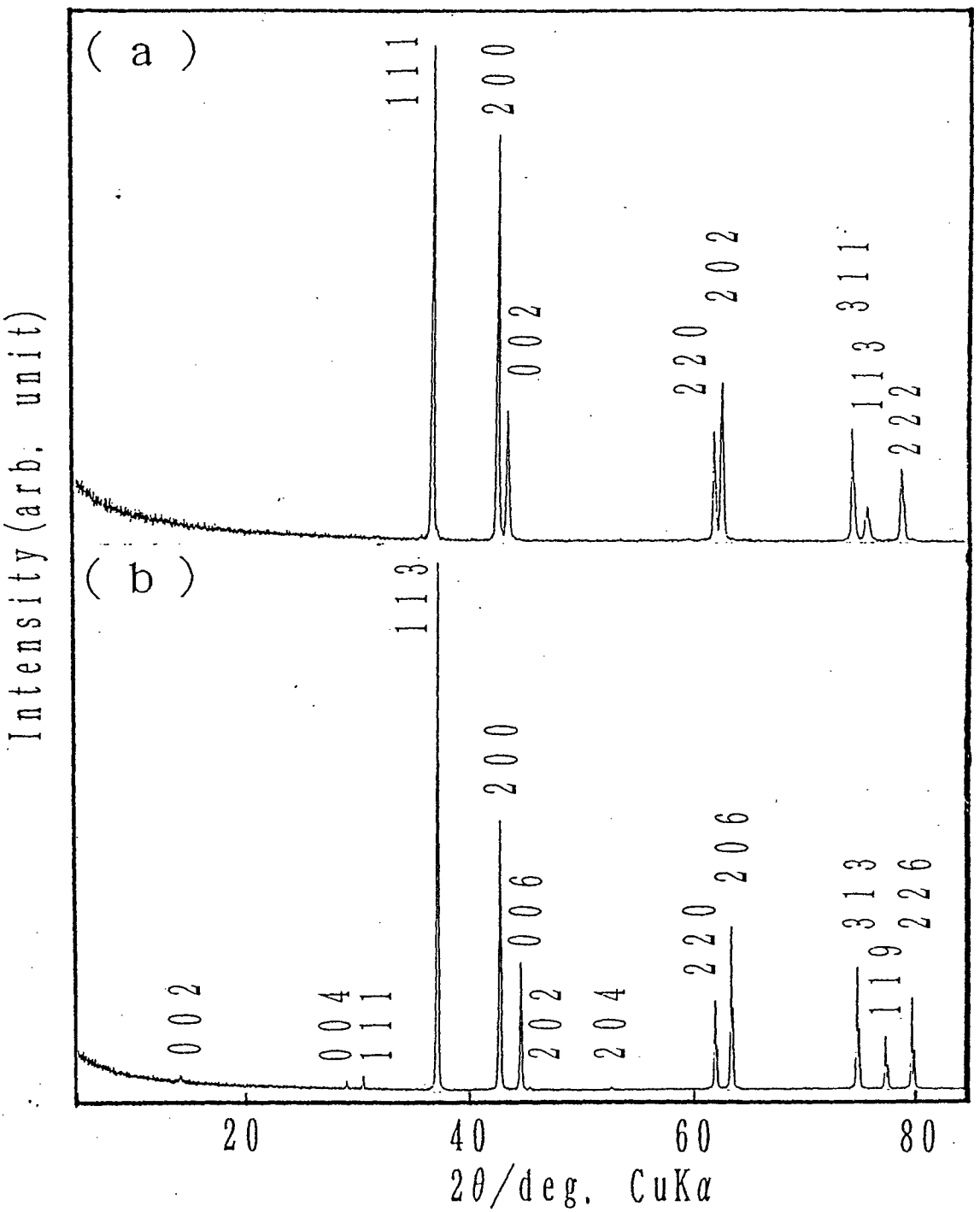


Fig. 1. Powder X-ray diffraction patterns of $Mn_6N_5$ (a) and $Mn_3N_2$ (b). In (a), all diffraction peaks were indexed as Mn taking fct cell ; a=0.4221nm, c=0.4137nm, c/a=0.980. In (b), all diffraction peaks were indexed as Mn taking three fold fct cell along c-axis direction ; a=0.4205nm, c=1.2128nm, c/a=0.961.

ructure transformation like order–disorder transition or fct–fcc transition such as $Mn_6N_5$ occurred in $Mn_3N_2$.

Fig. 2 depicts the temperature dependence of the magnetic susceptibilities $\chi$ of $Mn_6N_5$ and $Mn_3N_2$ from 100 to 958K on heating process. Values of $\sigma_s$ at room temperature of ferromagnetic impurity in $Mn_6N_5$ and $Mn_3N_2$ were estimated to be 0.025–0.031 and 0.030–0.084Gcm$^3$/g by extrapolation to a zero field from $\sigma$–$H$ curves, respectively. $T_c$ of the ferromagnetic impurity was observed to be about 740K indicating that the ferromagnetic impurity was $Mn_4N$ ($T_c$=738K, $\sigma_s$=27.0Gcm$^3$/g [2. 7, 10]). An amount of $Mn_4N$ in $Mn_3N_2$ or $Mn_6N_5$ was evaluated to be less than 0.3% by the values of $\sigma_s$. The magnetic susceptibilities of $Mn_6N_5$ and $Mn_3N_2$ were calculated after correcting the observed value with $\sigma_s$. The magnetic susceptibilities of $Mn_6N_5$ and $Mn_3N_2$ at 298K were $(10.6\pm0.2)\times10^{-6}$cm$^3$/g and $(7.5\pm0.5)\times10^{-6}$cm$^3$/g, respectively. That for $Mn_3N_2$ was close to the previously reported value of $9.2\times10^{-6}$cm$^3$/g [9].

As shown in Fig. 2, a slightly swelled part around 750K in the $\chi$–$T$ curve of $Mn_3N_2$ on heating was probably due to the small amount of $Mn_4N$ ($T_c$=738K) [2, 7, 10]. Except this region, $\chi$–$T$ curves indicate maxima in the temperature ranges of 655 to 660K for $Mn_6N_5$ and 914 to 936K for $Mn_3N_2$, respectively. The same maxima are also found in the $\chi$–$T$ curves on cooling in the temperature range of 627 to 636K and 859 to 869K for $Mn_6N_5$ and $Mn_3N_2$, respectively. It is found from the $\chi$–$T$ curves that the magnetism of both $Mn_3N_2$ and $Mn_6N_5$ is antiferromagnetic. This results on $Mn_3N_2$ is consistent with the magnetic structure of $Mn_3N_2$ [9]. Each maximum point in the $\chi$–$T$ curves of $Mn_6N_5$ and $Mn_3N_2$ was close to each phase transition temperature of 660–663K and 913–923K obtained by DTA, respectively. Therefore the temperatures at the maximum part in $\chi$–$T$ curves for them are not necessary their Néel temperature. However many evidences that the magnetic transition temperature is comparable to the phase transformation temperature have been observed, e.g. on $\gamma$–Mn [14–16], MnPt [17], $Mn_3GaN$ [18] CrN [19] and so

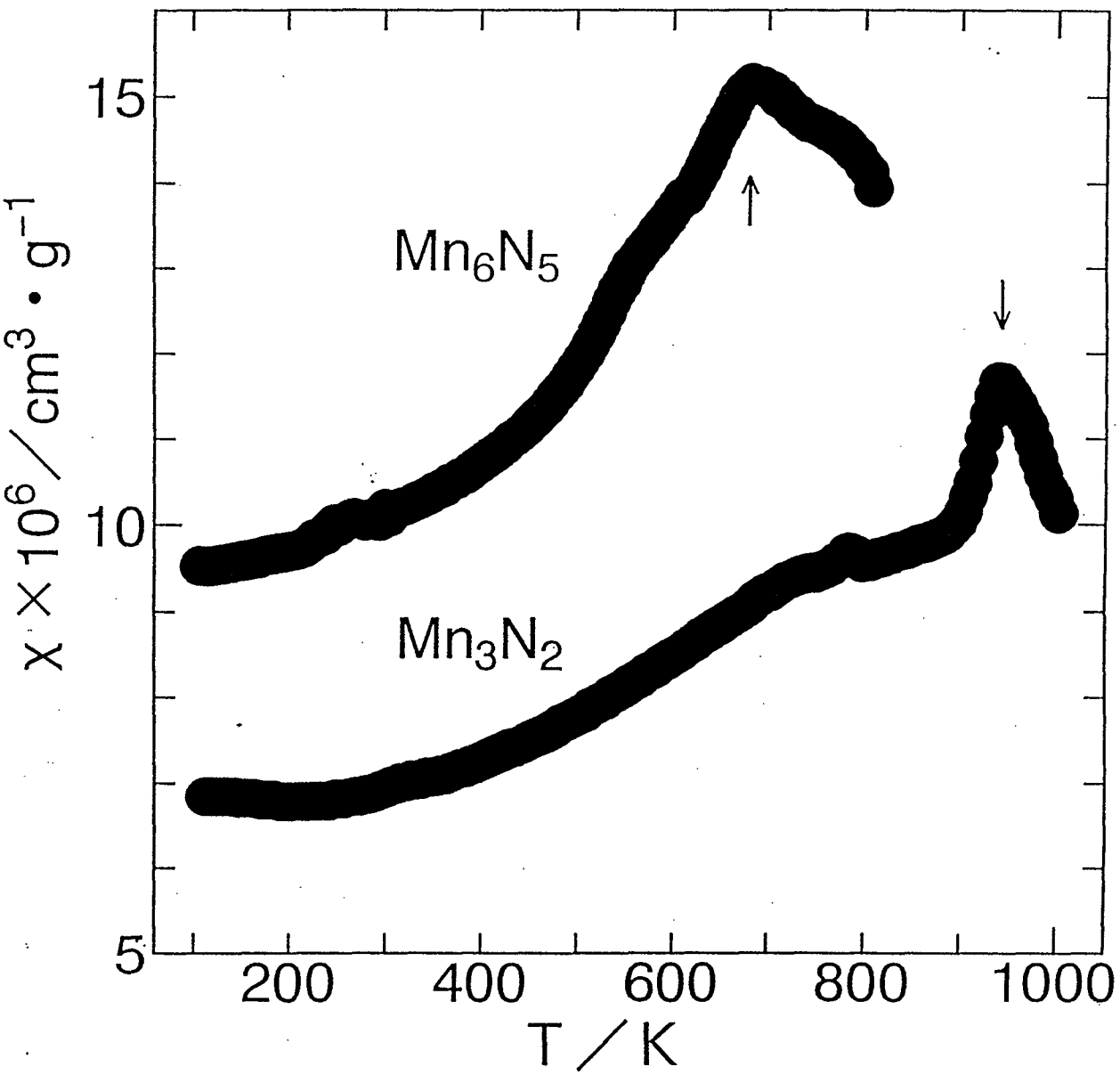


Fig. 2. Temperature dependence of magnetic susceptibility for $Mn_6N_5$ and $Mn_3N_2$. Arrows indicate the maximum point in $\chi$–$T$ curve. $\chi$ for $Mn_6N_5$ and $Mn_3N_2$ were obtained by correction of $\sigma_s$. $\sigma_s$ in $Mn_6N_5$ and $Mn_3N_2$ powder obtained from values of $\sigma$ extrapolated to zero magnetic field, $H$ in $\sigma$–$H$ curves at various temperatures, respectively, see text.

TABLE. 1 Crystal structure, shortest Mn–Mn distance $r_{Mn-Mn}$, magnetism, magnetic transition temperature $T_{mag}$, and magnetic moment per a Mn atom, $\mu_{Mn}$ for γ–Mn and $MnN_y$.

| Species | Crystal structure | $r_{Mn-Mn}$/nm | Magnetism | $T_{mag}$/K | $\mu_{Mn}/\mu_B$ |
|---|---|---|---|---|---|
| γ–Mn | fct (<480K)<br>fcc (>480K) | 0.2592 | Antiferro | 480 | 2.4 (0) at 0K |
| $Mn_4N$ | $Fe_4N$ type | 0.273 | Ferri | 738 | 3.85 (0)<br>–0.9 (2) at 77K |
| $Mn_2N$ | ζ–$Fe_2N$ type | 0.2797 | Antiferro | 301 | 1.6 (3) at 120K |
| $Mn_3N_2$ | Mn: fct at 295K<br>N : ordered | 0.2916 | Antiferro | ≧925±11 | 4.3 (2)<br>3.4 (5) at 11K |
| $Mn_6N_5$ | Mn : fct (<683±20K)<br>fcc (>683±20K)<br>N : ambiguous | 0.2955 | Antiferro | ≧655±3 | unknown |

The value of $r_{Mn-Mn}$ correspond to the shortest Mn–Mn distance in a plane parallel to the c–axis. In the $\mu_{Mn}$ column, the number of nitrogen atoms neighboring a Mn atom with the value of $\mu_{Mn}$, $z_N$ are designated in parentheses.

on. $Mn_6N_5$ and $Mn_3N_2$ as well as γ–Mn seem to take place the magnetic transition accompanied by the structural change. Néel temperatures of $Mn_6N_5$ and $Mn_3N_2$ were estimated to be 655–660K and 914–936K, respectively. Such the fact that each magnetic transition temperatures on cooling is lower than each on heating of $Mn_6N_5$ and $Mn_3N_2$, may reflect the hysteresis accompanying the structural change. In subsequent sections, the Néel temperatures of $Mn_6N_5$ and $Mn_3N_2$ on heating are used as magnetic transition temperature $T_{mag}$.

*3.2 Consideration with respect to magnetic properties of $MnN_y$ with $0<y<1$*

Though it was clarified that $Mn_4N$ possess the band like electronic structure, electronic structure of other $MnN_y$ is not still revealed. The magnetic transition temperature $T_{mag}$ is generally represented by molecular field theory based on localized spin model [20] as follows,

$$T_{mag} = \frac{2z|J_{M-M}|S(S+1)}{3k} \qquad (1).$$

Where $z$ represent the coordination numbers, $J_{M-M}$ is the exchange coupling constant between the nearest neighboring magnetic atoms, $S$ is spin quantum numbers, and $k$ is Boltzmann constant. In the case of 3d transition metal, the term $S(S+1)$ is equals to the square of magnetic moment per a metal atom, $\mu_M^2$.

$T_{mag}$ and $\mu_{Mn}$ of $MnN_y$ and γ–Mn are given in Table 1 with the shortest Mn–Mn distance, $r_{Mn-Mn}$ and with the crystal structure of them. The values of $r_{Mn-Mn}$ correspond to the shortest Mn–Mn distance in a plane parallel to the c–axis. Where the crystallographic data and magnetic properties of γ–Mn [14–16], $Mn_4N$ [2, 6, 7] and $Mn_2N$ [8], $\mu_{Mn}$ of $Mn_3N_2$ [9], and the phase transition temperature of $Mn_6N_5$ [13] were referred to those of published data.

The values of $r_{Mn-Mn}$ of γ–Mn and $MnN_y$ differed from each other in Table 1. As

the relation between $y$ and $r_{Mn-Mn}$ of $MnN_y$ ($0 \leqq y < 1$) was revealed, the $r_{Mn-Mn}$ for them were plotted against the nitrogen content $y$, as shown in Fig. 3. The $r_{Mn-Mn}$ of $Mn_{2-3}N$ were calculated from the lattice parameter of the previous data [5]. It is found from Fig. 3 that there is a linear relationship between $y$ and $r_{Mn-Mn}$ in spite of different crystal structure.

In order to discuss the variation of $T_{mag}$ with the $r_{Mn-Mn}$ for $MnN_y$, the magnetic transition temperature are plotted against each shortest M–M distance (M=Mn, Fe, Co) on $Mn_6N_5$, $Mn_3N_2$, $Mn_{2-3}N$ [1, 8], $Mn_4N$ [6, 7] and manganese alloys with fcc or fct lattice, such as γ–Mn [14–16], MnNi [17], MnPd [17], MnPt [17], CoMn [21], FeMn [22], $Mn_3Rh$ [23], $Mn_3Pt$ [23], $(CoMn)_{0.75}Fe_{0.25}$ [21], $Fe_{0.82}Mn_{0.14}C_{0.04}$ [24] and $Fe_{0.89}Mn_{0.07}C_{0.04}$ [24] as shown in Fig. 4 (a). Adachi *et al.* [21] found that $T_{mag}$ of disordered antiferromagnetic fcc alloys increase with increasing their lattice parameter. Their observation corresponds to the change of $T_{mag}$ against $r_{M-M}$ ranging from 0.25 to 0.257nm in Fig. 4 (a). The data of Mn alloys in Fig. 4 (a) are rather scattered, but there is obviously the trend that $T_{mag}$ of alloys with $r_{M-M}$<0.27nm increase with an increase in $r_{M-M}$, but $T_{mag}$ of the alloys with $r_{M-M}$>0.27nm decrease with increasing $r_{M-M}$. The $T_{mag}$ vs $r_{M-M}$ plots for $Mn_4N$, $Mn_3N_2$ and $Mn_6N_5$ with fct or fcc lattice are found to exist in a convex band appeared in the $T_{mag}$ vs $r_{M-M}$ plots for the Mn alloys. However, the $T_{mag}$ vs $r_{M-M}$ plots of $Mn_{2-3}N$ which have Mn lattice near to hcp deviate from the convex band for Mn alloys in Fig. 4 (a). By Cluster–Variation method on the basis of Ising model of ferromagnetism in fcc Pt–Mn alloys, Sato [25] found that $|J_{Mn-Mn}|$ became smaller with an increase in the ratio of atomic distance to d–shell radius, $r/R$. It is predicted by this concept and eq. (1) that $T_{mag}$ decrease monotonously with increasing $r_{M-M}$. However, the result shown in Fig. 4 (a) is inconsistent with the above prediction. Some factors other than $|J_{M-M}|$ are required to interpret the tendency in the $T_{mag}$ vs

$r_{M-M}$ plot.

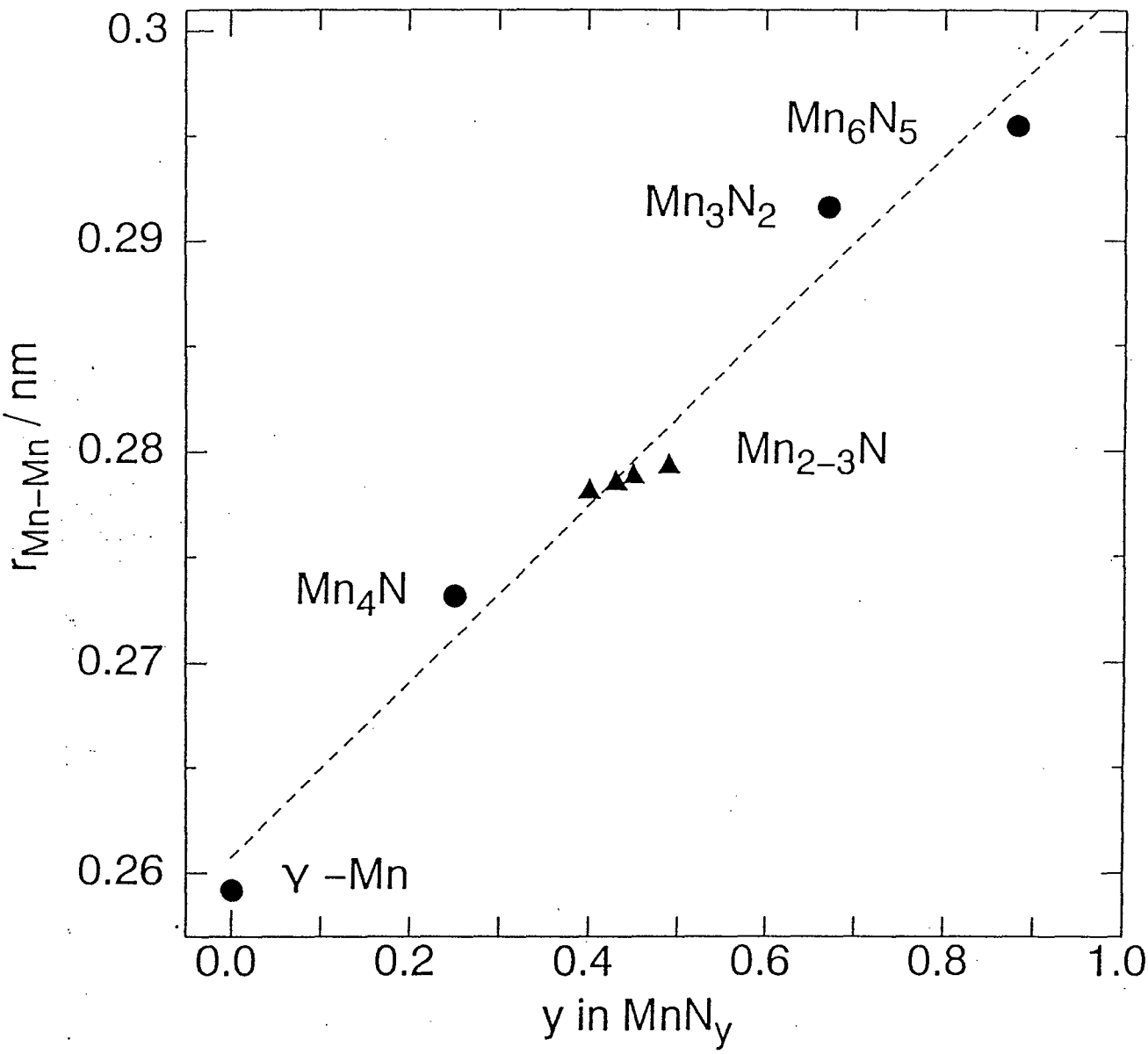


Fig. 3. The relation between nitrogen content $y$ and the shortest Mn–Mn distance, $r_{Mn-Mn}$. Closed circle denotes that Mn has fcc or fct lattice, and closed triangle denotes that Mn takes hcp lattice. The values of $r_{Mn-Mn}$ correspond to the shortest Mn–Mn distance in a plane parallel to the c–axis. The dashed line indicates the line obtained by least square fitting between $y$ and $r_{Mn-Mn}$ with 0.986 of correlation coefficient.

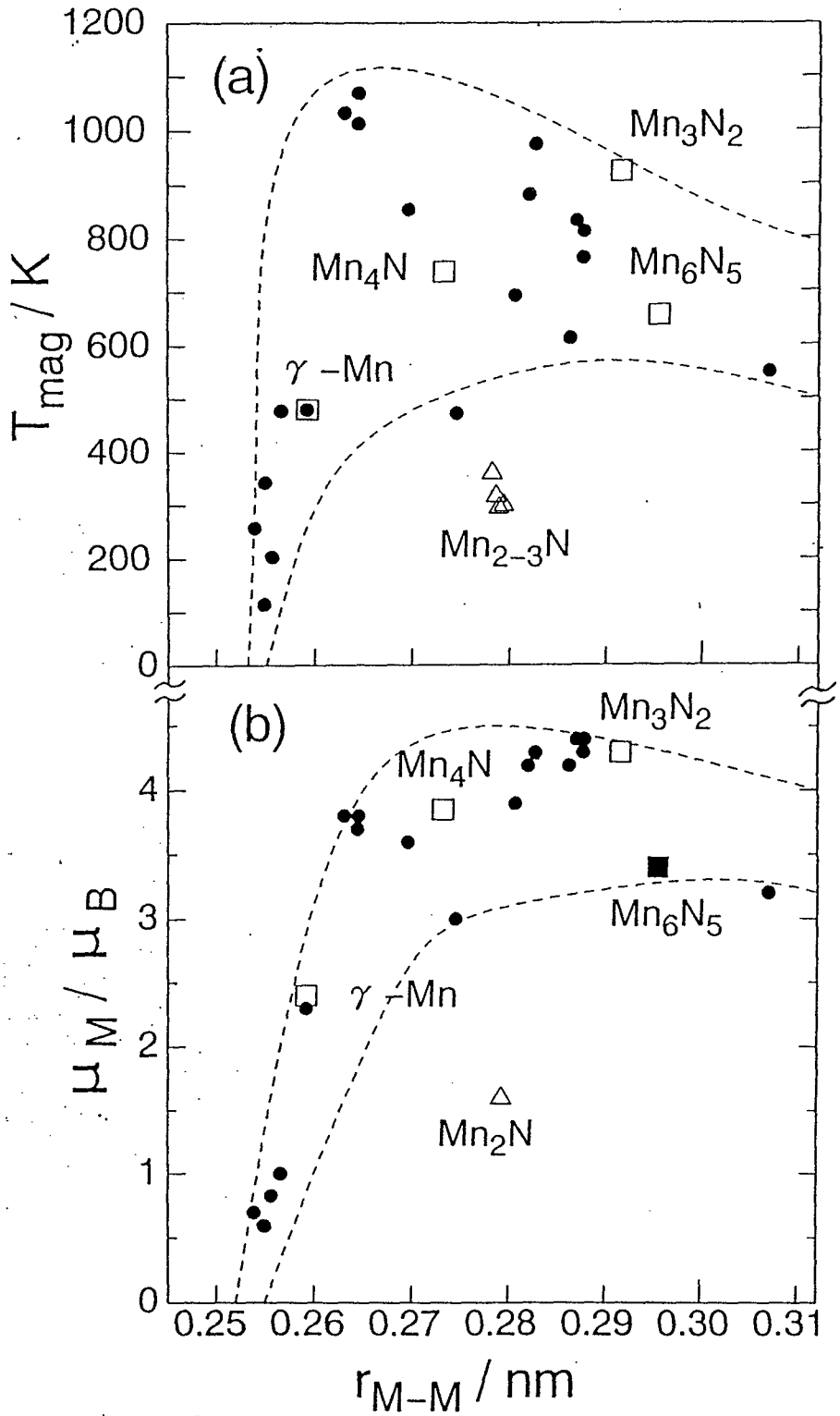


Fig. 4. Plots of magnetic transition temperature $T_{mag}$ (a) and magnetic moment per a metal atom $\mu_M$ (b) against the shortest M–M distance $r_{M-M}$ (M=Mn, Fe and Co) for $MnN_y$ and Mn alloys with fcc or fct lattice. Small circle denotes $T_{mag}$ vs $r_{M-M}$ or $T_{mag}$ vs $r_{M-M}$ plots for Mn alloys. In Fig. 4 (a), the values of $r_{Mn-Mn}$ for $MnN_y$ was taken from Table. 1 and $T_{mag}$ vs $r_{Mn-Mn}$ plots for $Mn_{2-3}N$ were from previous data. The part which is surrounded with dashed lines in Fig. 4 (a), shows the correlation between $T_{mag}$ and $r_{M-M}$. The larger value of $\mu_{Mn}$ as shown in Table. 1 utilizes as $\mu_{Mn}$ of each $Mn_4N$ and $Mn_3N_2$. The part which is surrounded with dashed lines in Fig. 4 (b) exhibits the correlation between $\mu_M$ and $r_{M-M}$.

According to eq. (1), the magnetic moment per a M atom (M=Mn, Fe, Co), $\mu_M$ is thought as a factor responsible for $T_{mag}$ of $MnN_y$ and alloys. The magnetic moments of a M atom in $MnN_y$ and the manganese alloys with fcc or fct lattice are plotted against the $r_{M-M}$ in Fig. 4 (b). The value of $\mu_{Mn}$ for $Mn_6N_5$ was estimated to be $3.4\mu_B$ [9] which correspond to smaller one of $\mu_{Mn}$ ($z_N$=5) for $Mn_3N_2$ in Table. 1, because a Mn atom in $Mn_6N_5$ with tetragonally distorted NaCl structure [9, 13] have probably five nearest neighboring nitrogen atoms. In both cases of $Mn_4N$ and $Mn_3N_2$, Mn atoms with two different lattice sites has been observed as shown in Table 1. The magnetic moment of the Mn atom with smaller N-coordination number $z_N$ is larger than that of Mn atom with larger N-coordination number. The value of $\mu_{Mn}$ in $MnN_y$ may be affected by the formation of Mn-N bond and also by the expansion and deformation of lattice accompanied by an increase in its nitrogen content. Such facts were observed previously in Fe-N and Fe-C system. In α'-martensite [26], though the magnetic moment of Fe atom adjacent to nitrogen or carbon atoms decrease by the formation of Fe-N and Fe-C bonds, those of the second or third neighboring Fe atoms also increase by the expansion and deformation of lattice. Nakajima *et al.* [27] found that Fe atoms at remoter lattice sites from nitrogen atoms in $Fe_{16}N_2$, have the larger magnetic moments. The mechanism which $\mu_{Fe}$ of a Fe atom with smaller N-coordination number is larger than that of a Fe atom with larger N-coordination number will be described by exemplifying $Fe_4N$ in appendix. Sakuma [28] calculated the density of state for $Fe_4N$, $Fe_3N$ and $Fe_{16}N_2$ using the linearized muffin-tin orbital (LMTO)-the atomic sphere approximation (ASA) method and concluded that the N atom is to bring about the large magnetic moments through lattice expansion (magnetovolume effect) and prevent the exchange-splitting by promoting the itineracy of electrons. If the larger $\mu_{Mn}$ were used for $Mn_4N$ and $Mn_3N_2$, the relation between $\mu_{Mn}$ and $r_{Mn-Mn}$ is similar to that between $T_{mag}$ and $r_{M-M}$. However, a remarkable deviation from the tendency in the $\mu_M$ vs $r_{M-M}$ plot is observed using the small and

averaged $\mu_{Mn}$ for $Mn_4N$ and $Mn_3N_2$. Consequently, the large $\mu_{Mn}$ for $Mn_4N$ and $Mn_3N_2$ were adopted in the $\mu_M$ vs $r_{M-M}$ plot in Fig. 4 (b).

From Fig 4, $\mu_M$ was presumed to contribute more greatly to $T_{mag}$ than $|J_{M-M}|$ of $MnN_y$ and Mn alloys. In the case of Mn alloys, $T_{mag}$ is sensitively affected by the coordination number of magnetic atoms and the degree of ordering of Mn and non-magnetic atoms, depending on chemical composition of Mn alloys. Therefore, the relation between $T_{mag}$ and $\mu_M$ is shown only for $MnN_y$ in which each Mn is surrounded with 12 neighboring Mn atoms.

Fig. 5 depicts $T_{mag}$ vs $\mu_{Mn}$ plots for γ-Mn and $MnN_y$. Here, larger magnetic moments were used as $\mu_{Mn}$ for $Mn_4N$ and $Mn_3N_2$. It was found that there is a obviously linear relationship between the $T_{mag}$ and the $\mu_{Mn}$. Probably, $T_{mag}$ of $MnN_y$ depend on the value of $\mu_{Mn}$ of the Mn atoms with smaller N-coordination number as can be seen from Table 1.

A linear relation between magnetic moments per a metal atom and the magnetic transition temperature were observed at the Cr base alloys which contain 1 at% of V, Mo, W, Mn, Ru and Re, respectively [29]. It has been reported also in Mn-Ni alloy [30] that the $\mu_{Mn}$ and $T_N$ of Mn-Ni alloy decrease linearly with increasing Ni content. The linear relationships in $T_N$-$\mu_{Mn}$ plots have been reported only in the range of 1.7 to 2.4$\mu_B$, so far [30]. The most interesting aspect of present result is that the linear relationship between $T_{mag}$ and larger $\mu_{Mn}$ is kept over the wide range from about 1.6 to 4.3$\mu_B$, though the reason why the $T_{mag}$ for $MnN_y$ depends on larger $\mu_{Mn}$ is still unresolved. The relationship between the magnetic transition temperature and the larger magnetic moment for $MnN_y$ may be interpreted by clarifying their electronic structure through band calculation.

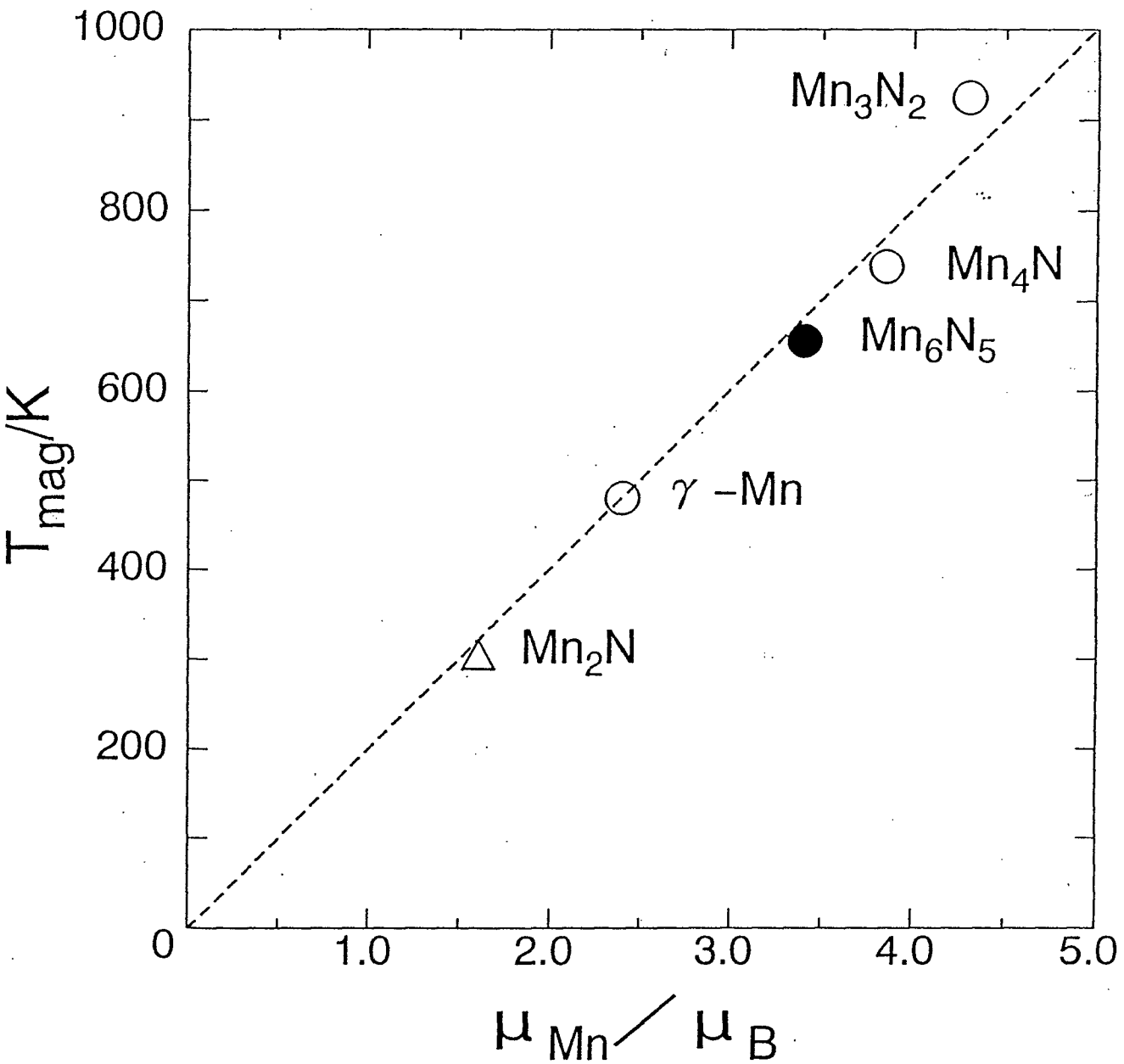


Fig. 5. The relation between larger magnetic moments $\mu_{Mn}$ and magnetic transition temperature $T_{mag}$ for $MnN_y$ with $0 \leqq y < 1$. The dashed line indicates the line obtained by least square fitting between $\mu_{Mn}$ and $T_{mag}$ with 0.994 of correlation coefficient. The magnetic moment in $Mn_6N_5$ was assumed to be $3.4\mu_B$ corresponding to that of the Mn atom surrounding with five nitrogen atoms in $Mn_3N_2$ as shown in Table 1.

*4. Summary*

The magnetic susceptibility measurements for $Mn_6N_5$ and $Mn_3N_2$ prepared by nitriding α–Mn powder in $NH_3$ flow were carried out between 100 and 958K to clarify the magnetic properties of manganese nitrides. The magnetism of both $Mn_6N_5$ and $Mn_3N_2$ are antiferromagnetic below 655–660 and 914–936K, respectively, and their antiferromagnetic interaction disappeared with accompanying the phase transition. The change of $T_{mag}$ with $r_{M-M}$ was found to correspond considerably to that of $\mu_M$ with $r_{M-M}$ of $MnN_y$ and Mn alloys. Linear relationship between $T_{mag}$ and larger $\mu_{Mn}$ of $MnN_y$ with $0 \leqq y < 1$ obtained experimentally.

*Appendix*

The crystal structure of $Fe_4N$ is shown in Fig. 1 (a) of chapter 1. It can be visualized as an fcc Fe lattice with an additional N atom at the center of the cell. Whereas only one Fe sublattice is observed in fcc Fe (γ–Fe), two Fe sublattice can be accounted for in $Fe_4N$; (i) the Fe atoms at the cube corner positions (hereafter referred to as Fe(1)); (ii) the Fe atoms at the face center positions (hereafter referred to as Fe(2)). The crystallographic position of N lead to six Fe(2)–N distances shorter than eight Fe(1)–N ones ($d$(Fe(2)–N)≈0.190nm; $d$(Fe(1)–N)≈0.329nm). These geometrical considerations suggest that Fe–N interactions would preferentially occur between face–center Fe and central N atoms rather than between corner Fe and N atoms.

The magnetism of $Fe_4N$ has been reported to be ferromagnetic with $T_c$ of 761K [2] and two different values of $\mu_{Fe}$ have been observed [3] ($\mu_{Fe(1)}=3\mu_B$; $\mu_{Fe(2)}=2\mu_B$). The occurrence of two different $\mu_{Fe}$ can be explained the following mechanism [31, 32].

Fig. 6 depicts the changes of the local densities of states $D(E)$ of Fe 3d bands at Fe(2) (a) and Fe(1) (b) in $Fe_4N$, accompanying the Fe–N interaction, respectively. N 2p bands are situated in the top of the partially filled Fe(2) 3d band and overlap with them. p–d

mixing occur mainly between N 2p and Fe(2) 3d bands. The level repulsion due to the p–d mixing will cause a downward shift in energy of the *D(E)* of Fe(2) 3d band in the down spin state to place them lower than the *D(E)* of Fe(1) atoms more distant from the N site. In other words, the *D(E)* of Fe(2) atoms in down spin state are changed from dotted lines to solid ones with the Fe–N interactions. The degree of the shift in *E* of *D(E)* of Fe 3d band in the down spin state is larger than that of Fe 3d band in the up spin state, because Fe 3d band in down spin state possess more 3d holes than that in the up spin state. Accompanying the energy shift of Fe(2) 3d band, the center of *D(E)* of Fe(1) atoms in down spin state shift toward relatively high energy position. That is, the *D(E)* of Fe(1) atoms in down spin state is changed from dotted lines to solid ones. The electron transfer from the Fe(1) 3d bands to the Fe(2) ones result from the shift of that of Fe(1) atoms in down spin state. As a result, the local magnetic moment of a Fe(1) atoms raised, while that of a Fe(2) atom is lowered.

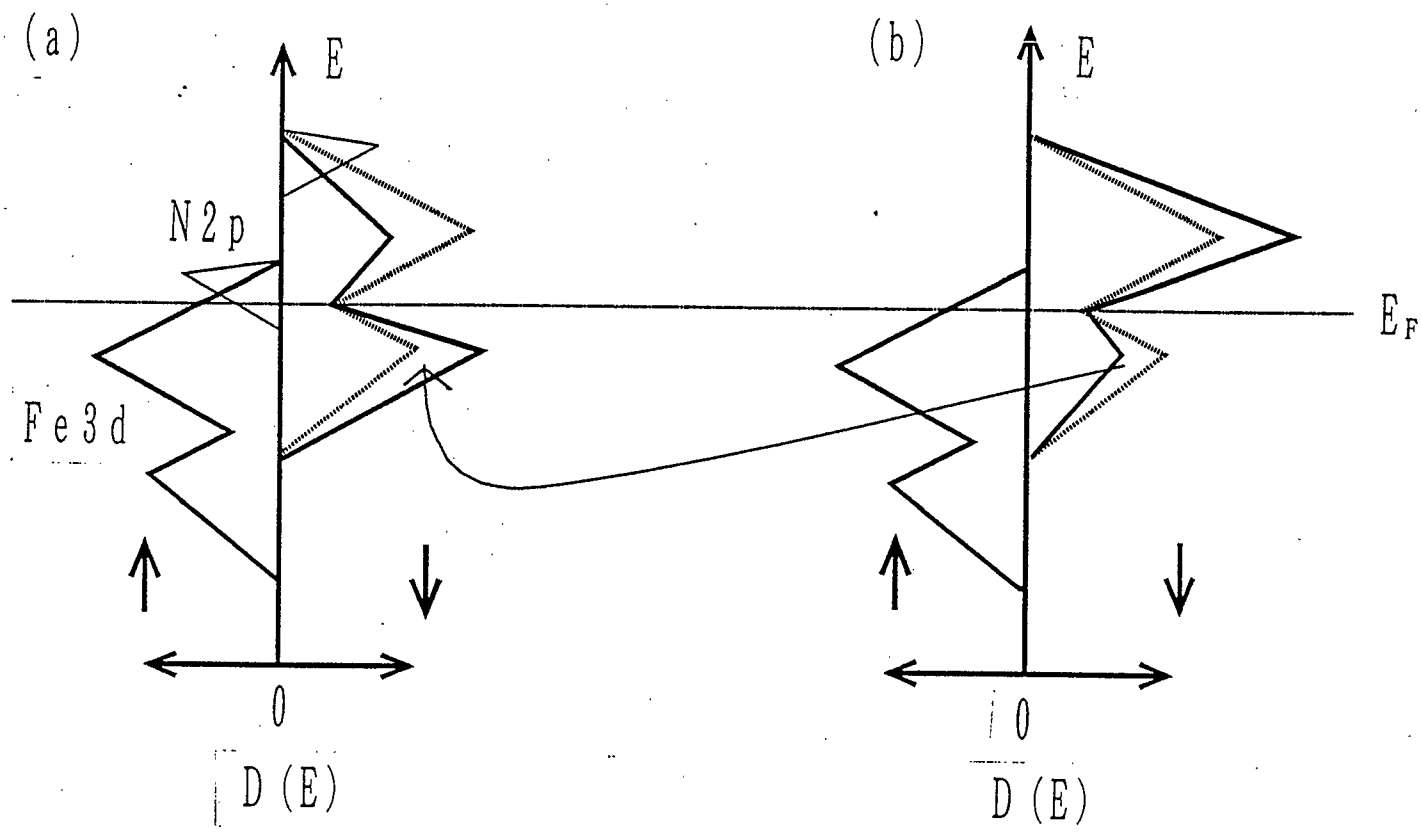


Fig. 6. The local densities of states (*D(E)*) of N 2p band and Fe 3d bands in $Fe_4N$ at the face center positions (Fe(2)) (a), and at the cube corner ones (Fe(1)) (b) [31]. *D(E)* of Fe(1) and Fe(2) atoms are changed from dotted lines to solid ones with the inclusion of N atoms, and the electrons of down spin states are then transferred from Fe(1) 3d bands to Fe(2)ones. As a result, $\mu_{Fe}$ of a Fe(1) atom is raised, while that of a Fe(2) atom is lowered.

*References*


1 M. Mekata, H. Yoshimura and H. Takaki, *J. Phys. Soc. Jpn., 33* (1972) 62.

2 G. W. Wiener and J. A. Berger, *J. Met., 7* (1955) 360.

3 B. C. Frazer, *Phys. Rev., 112* (1958) 751.

4 M. Takahashi, H. Fujii, H. Nakagawa, S. Nasu and F. Kanamaru, *Proc. 6th International Conference on Ferrites,* The Japan Society of Powder and Powder Metallurgy, Tokyo and Kyoto, 1992, pp. 508.

5 N. A. Gokcen, *Bull. Alloy Phase Diagrams, 11* (1990) 33.

6 W. J. Takei, R. R. Heikes and G. Shirane, *Phys. Rev., 125* (1962) 1893.

7 M. Mekata, *J. Phys. Soc. Jpn., 17* (1962) 796.

8 M. Mekata, J. Haruna and H. Takaki, *J. Phys. Soc. Jpn., 25* (1968) 234.

9 G. Kreiner and H. Jacobs, *J. Alloys Comp., 183* (1992) 345.

10 Nippon Kagakukai (eds.), *Kagakubinran Kisohen* II, 3rd Ed, Maruzen, (1984) pp. 510.

11 H. Jacobs and C. Stübe, *J. Less-Common Met., 96* (1984) 323.

12 F. Lihl, P. Ettmayer and A. Kutzelnigg, *Z. Metallkd., 53* (1962) 715.

13 N. Ōtsuka, Y. Hanawa and S. Nagakura, *Phys. Status Solidi A, 43* (1977) K127.

14 Y. Endoh and Y. Ishikawa, *Kotai Butsuri, 5* (1970) 245.

15 G. E. Bacon, I. W. Dunmur, J. H. Smith and R. Street, *Proc. R. Soc. London A., 241* (1957) 223.

16 D. Maneghetti and S. S. Sidhu, *Phys. Rev., 105* (1957) 130.

17 L. Pál, E. Krén, G. Kádár, P. Szabó and T. Tarnóczi, *J. Appl. Phys., 39* (1968) 538.

18 R. Navarro, J. A. Rojo, J. García, D. González, J. Bartoromé and Ph. L'Héritier, *J. Magn. Magn. Mater., 59* (1986) 221.

19 L. M. Corliss, N. Elliott and J. M. Hastings, *Phys. Rev., 117* (1960) 929.

20 S. Chikazumi, K. Oota, K. Adachi, N. Tsuda and Y. Ishikawa (eds.), *Jiseitai handbook*, Asakura-shoten (1975) pp. 54.

21 K. Adachi, K. Sato, M. Matsui and S. Mitani, *J. Phys. Soc. Jpn., 35* (1973) 426.

22 Y. Ishikawa and Y. Endoh, *J. Phys. Soc. Jpn., 23* (1967) 205.

23 E. Krén, L. Pál, G. Kádár, P. Szabó and T. Tarnóczi, *Phys. Rev., 171* (1968) 574.

24 Y. Endoh and Y. Ishikawa, *J. Phys. Soc. Jpn., 30* (1971) 1614.

25 H. Sato, *J. Appl. Phys., 31* (1960) 327S.

26 K. Mitsuoka, H. Miyajima, H. Ino and S. Chikazumi, *J. Phys. Soc. Jpn., 53* (1984) 2381.

27 K. Nakajima, S. Okamoto, M. Tanaka and H. Sekizawa, *Nippon Oyo Jiki Gakkaishi, 15* (1991) 703.

28 A. Sakuma, *J. Magn. Magn. Mater., 102* (1991) 127.

29 W. C. Koehler, R. M. Moon, A. L. Trego and A. R. Mackintosh, *Phys. Rev., 151* (1966) 405.

30 H. Uchishiba, *J. Phys. Soc. Jpn., 31* (1971) 436.

31 A. Sakuma, *Nippon Oyo Jiki Gakkaishi, 17* (1993) 741.

32 J. Kanamori, *Prog. Theor. Phys. Suppl., 101* (1990) 1.

## Chapter 3 Application of the relation between the magnetic moment and the magnetic transition temperature to $MN_y$ besides $MnN_y$

3d Metal atoms in 3d metal nitrides often distribute at different lattice sites which take different N–coordination number each other. In such a case, magnetic moment of metal atoms in a nitride varies with depending on N–coordination number of metal atom ($z_N$), i.e. the metal atom with larger N–coordination number possesses smaller magnetic moment. A linear relationship between the magnetic transition temperature ($T_{mag}$) and the largest magnetic moment ($\mu_{(max)}$) of metal atoms in metal nitride was found out in the Mn and N system as described in chapter 2.

It is interesting whether the linear correlation can apply to other metal nitrides $MN_y$ besides $MnN_y$ or not. To examine of the linear correlation between $\mu_{M(max)}$ and $T_{mag}$, $MN_y$ with the ordered arrangement of N atoms are desired.

$CrN_y$ are unsuitable for this purpose, because all Cr atoms occupy the same lattice site in both Cr [1] and CrN [2]. The values of $\mu_{M(max)}$ and $T_{mag}$ of metal nitrides with ordered arrangement of N such as $Co_4N$ and $Ni_4N$ are not yet decided. The magnetic data of $CoN_y$ and $NiN_y$ are insufficient to examine the relation between $\mu_{M(max)}$ and $T_{mag}$.

On the other hand, there are many data about the magnetism of $FeN_y$ in analogy with $MnN_y$ as shown in Table 2 of chapter 1. Each of crystal phases such as $Fe_4N$ [3], $Fe_{16}N_2$ [4] and $Fe_2N_{0.78}$ [5] with the ordered structure of nitrogen atoms, possess the two or three kinds Fe atoms with different $\mu_{Fe}$. In $Fe_4N$ and $Fe_2N_{0.78}$, the $\mu_{Fe}$ of the Fe atom with smaller N–coordination number is larger than that of the Fe atom with larger one. In $Fe_{16}N_2$, the first neighbor Fe atom of nitrogen has the least magnetic moment, and the third one has the maximum moment. Consequently, the relation between $T_{mag}$ and $\mu_{Fe(max)}$ in $FeN_y$ is examined. Fig. 1 depicts the plots of $T_{mag}$ against $\mu_{Fe(max)}$ of γ–Fe (fcc), ε–Fe and $FeN_y$ ($0<y<0.5$) with the hcp or fcc lattice of M atoms. $T_{mag}$ and $\mu_{Fe}$ of α–Fe γ–Fe [7], ε–Fe [8], $Fe_{2.04}N$ [8], $Fe_{2.5}N$ [5, 8] and $Fe_4N$ [3, 9] are previous data. In the case of

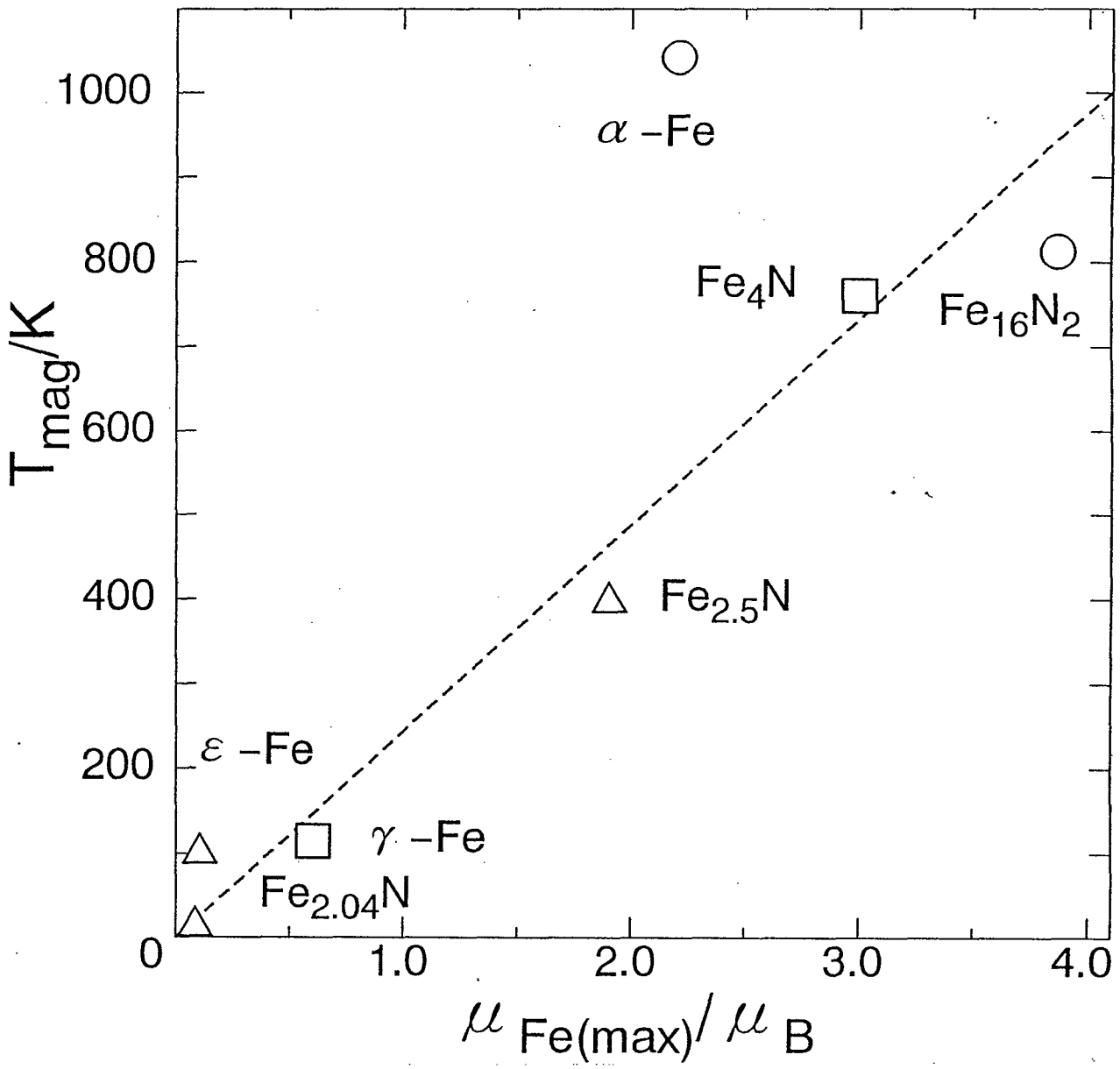


Fig. 1. Relation between the largest magnetic moment per a Fe atom ($\mu_{Fe(max)}$) and the magnetic transition temperature ($T_{mag}$) for α–Fe (bcc) [6], γ–Fe (fcc) [7], ε–Fe (hcp) [8], $Fe_4N$ [3, 10], $Fe_{2.5}N$ [5, 9], $Fe_{2.04}N$ [9] with fcc or hcp lattice of Fe atoms and $Fe_{16}N_2$ [4] with bct Fe lattice. The dashed line was obtained by least square fitting for $FeN_y$ with fcc or hcp Fe lattice between $\mu_{Fe}$ and $T_{mag}$ with 0.985 of correlation coefficient. Open circles, triangles and squares denote close–bcc, hcp and fcc arrangement of Fe atoms, respectively.

$Fe_4N$ and $Fe_{2.5}N$, the values of the largest $\mu_{Fe}$ were adopted. It is found that $T_{mag}$ changes linearly with $\mu_{Fe(max)}$ in γ–Fe, ε–Fe and $FeN_y$ in a similar manner to as γ–Mn and $MnN_y$. However, the $T_{mag}$ vs $\mu_{Fe(max)}$ plots for α–Fe and $Fe_{16}N_2$ with bcc or bct Fe lattice as the primitive structure deviated considerably from the linear relation between $T_{mag}$ and $\mu_{Fe(max)}$ as shown in Fig. 1. The deviation from the linear relationship in the $T_{mag}$ vs $\mu_{Fe(max)}$ plots for $Fe_{16}N_2$ and α–Fe may be attributed to the difference in Fe–coordination number of the Fe atom between the crystal phases of $FeN_y$. That is, it is shown that the linear relation between $T_{mag}$ and $\mu_{Fe(max)}$ are only maintained in $FeN_y$ with the nearly close–packed structure of Fe atoms such as hcp or fcc. It is found that the linear correlation in the $T_{mag}$ vs $\mu_{Fe(max)}$ plot, which was observed in $MnN_y$, can apply to $FeN_y$ with close–packed structure of Fe atoms.

*References*


1 W. C. Koehler, R. M. Moon, A. L. Trego and A. R. Mackintosh, *Phys. Rev., 151* (1966) 405.

2 L. M. Corliss, N. Eliott and J. M. Hastings, *Phys. Rev., 117* (1960) 929.

3 B. C. Frazer, *Phys. Rev., 112* (1958) 751.

4 K. Nakajima, S Okamoto M. Tanaka and H. Sekizawa, *Nippon Oyo Jiki Gakkaishi, 15* (1991) 703.

5 K. H. Eickel and W. Pitsch, *Phys. Status Solidi, 39* (1970) 121.

6 S. Chikazumi, K. Oota, K. Adachi, N. Tsuda and Y. Ishikawa (eds.), "*Jiseitai Handbook*", (Asakura-shoten) (1975) pp .

7 Y. Endoh and Y. Ishikawa, *J. Phys. Soc. Jpn., 30* (1971) 1614.

8 H. Ohno, *J. Phys. Soc. Jpn., 31* (1971) 92.

9 M. Mekata, H Yoshimura and H Takaki, *J. Phys. Soc. Jpn., 33* (1972) 62.

10 G. W. Wiener and J. A. Berger, *J. Met., 7* (1955) 360.

## Chapter 4 Preparation and magnetic properties of cobalt nitrides $CoN_y$ and nickel nitrides $NiN_y$ (0<y<0.5)

### 1. *Introduction*

There are four crystal phases, $Co_4N$, $Co_3N$, $Co_2N$ and CoN in the cobalt and nitrogen system. $Co_4N$ with an antiperovskite type structure, which is isostructural to $Fe_4N$ [1], can be obtained only non-thermoequilibrium processes such as reactive sputtering method [2]. Both $Co_3N$ and $Co_2N$ possess the basic structure of hcp arrangement of metal atoms like $Fe_{2-3}N$ and $Fe_2N$ [3]. The fine Co powder obtained by reduction of $Co_3O_4$ in $H_2$ flowing in the temperature region between 623 and 673K, can convert to $Co_3N$ and $Co_2N$ in $NH_3$ flow at temperatures of 653 to 663K [3]. CoN with NaCl type structure was synthesized by thermal decomposition of $Co(NH_2)_3$ in vacuo in the temperature region between 323 and 343K [4] and CoN with a zinkblende structure was prepared by the non-explosive decomposition of $[Co(NH_3)_6](N_3)_3$ in the temperature region between 368 and 423K in vacuo [5].

Recently, the magnetic properties (saturation magnetization, coercivity and perpendicular magnetic anisotropy) of sputter-synthesized Co-N films were studied for use as media for high density magnetic recording [6-8]. However, the magnetism of individual $CoN_y$ phases was not so clearly analyzed in these studies. Oda *et al.* [2] presented that saturation magnetization of $Co_4N$ films were 46.5-85.1$Gcm^3/g$ at room temperature. The magnetism of $Co_3N_{1.55}$ has been reported to be antiferromagnetic below 11K [9].

There are several phases of nickel nitrides $NiN_y$ such as $Ni_4N$, $Ni_3N$, $Ni_2N$ and $Ni_3N_2$. $Ni_3N$ with a hexagonal structure which is analogous to $Co_3N$ and $Fe_{2-3}N$ could be only obtained by nitrizing Ni powder in $NH_3$ flow. Dorman and Sikkens [10] prepared $Ni_4N$, $Ni_3N$ and $Ni_2N$ films by reactive sputtering using Ni target and an Ar-$N_2$ gas

mixture. $Ni_4N$ are a fcc [10, 11] or a fct [10, 12] phases and are metastable above about 523K [13]. $Ni_2N$ with a bct unit cell is only obtained by reactive sputtering method [10]. The presence of $Ni_3N_2$ is quite unlikely [14, 15]. The magnetism of $Ni_3N$ has been referred to be non-ferromagnetic or paramagnetic [16-18] but has not been clarified in detail.

Mekata *et al.* [19] reported that hexagonal ($M_{2-3}N$) and orthorhombic ($M_2N$) nitrides such as $V_{2-3}N$, $Cr_{2-3}N$, $Mn_{2-3}N$, $Fe_{2-3}N$ and $Fe_2N$ were similar to their mother metals in magnetisms, but magnetic moment of these nitrides was reduced by producing metal-nitrogen bonding. However, the influences of the number of valence electrons of a M atom (*e/a*) on the magnetic properties of $M_{2-3}N$ and $M_2N$ have not been investigated so far. In this chapter, $Co_3N$, $Co_2N$ and $Ni_3N$ were prepared by thermal decompositions of $CoCl_2$ and $NiCl_2$ in $NH_3$ flow. Magnetic susceptibility ($\chi$), for them were measured in the temperature region between 83 and 298K to reveal their magnetic properties. Magnetic properties of $M_{2-3}N$ and $M_2N$ (M=Mn, Fe, Co, Ni) were studied in relation to the number of valence electrons per a M atom. Finally one of the role of nitrogen in the magnetisms of $M_{2-3}N$ and $M_2N$ were considered.

## 2. *Experimental*

$Co_3N$ and $Co_2N$ powder were obtained by thermal decomposition of about 0.1g and 0.05g of $CoCl_2$ (anhydrous, Nakarai Tesque) at 663K for 12h in $NH_3$ flow and at 663K for 2.5h in the same atmosphere, respectively, and samples were quenched to room temperature after heating. About 0.1g of $NiCl_2$ converted to $Ni_3N$ at 623K for 20h in $NH_3$ flow.

The identification of products were carried out using a X-ray diffractmeter (Rigaku Rotaflex/RINT CuK$\alpha$ radiation). The lattice parameters of products were obtained from X-ray diffraction (XRD) measurements using silicon as an internal standard. The nitrogen

and carbon contents in products were determined by thermal conductivity method (240C, Perkin Elmer Co.) and the chroline contents in them were analyzed by Stragand's method (MX–3 Yanagimoto Seisakusho).

Temperature dependence of magnetic susceptibilities ($\chi$) of the samples was measured at 12.5kOe by magnetic balance (MB–3, Shimazu Co.) between 83 and 298K in He atmosphere. Mn Tutton's salt was used as the standard substance of $\chi$. Temperature was calibrated by values of $\chi$ for Mn Tutton's salt at various temperatures. The magnetic field (*H*) dependence of magnetization ($\sigma$) for samples was measured in the magnetic field between 1.8 and 12.5kOe to evaluate the spontaneous magnetization $\sigma_s$ of some ferromagnetic impurity.

## 3 *Results and discussion*

### 3.1 *Structure and composition of $Co_3N$, $Co_2N$ and $Ni_3N$*

Fig. 1 shows the XRD patterns of $Co_3N$ and $Co_2N$. XRD patterns of $Co_3N$ and $Co_2N$ were indexed by using a hexagonal (a=0.4608nm, c=0.4361nm) and an orthorhombic (Pnnm [20], a=0.2853nm, b=0.4606nm and c=0.4305nm) unit cells, respectively. Lattice parameters of both $Co_3N$ and $Co_2N$ agreed with previous data [3, 20]. The relation between hcp arrangement of Co atoms and both unit cells of $Co_3N$ and $Co_2N$ were shown in Fig. 2 (a) and (b), respectively. The relations between the cell dimensions of $Co_3N$ and $Co_2N$, and those of the hcp arrangements of Co atoms were as follows, $a \approx \sqrt{3}a_0$ and $c \approx c_0$ in $Co_3N$, and $a \approx a_0$, $b \approx \sqrt{3}a_0$ and $c \approx c_0$ in $Co_2N$, respectively. It is implied that N atoms in $Co_3N$ and $Co_2N$ occupy regularly the octahedral interstitial sites in hcp Co structure. Such the regular occupation of N atoms have been observed in $Fe_2N$, $Fe_{2-3}N$ and $Ni_3N$ [17]. The crystal structure of $Co_2N$ was reported to be $CaCl_2$ antitype [20]. An ordered arrangement of N atoms in $Co_2N$ result in an orthorhombically deformed cell of a $CaCl_2$ antitype cell [20].

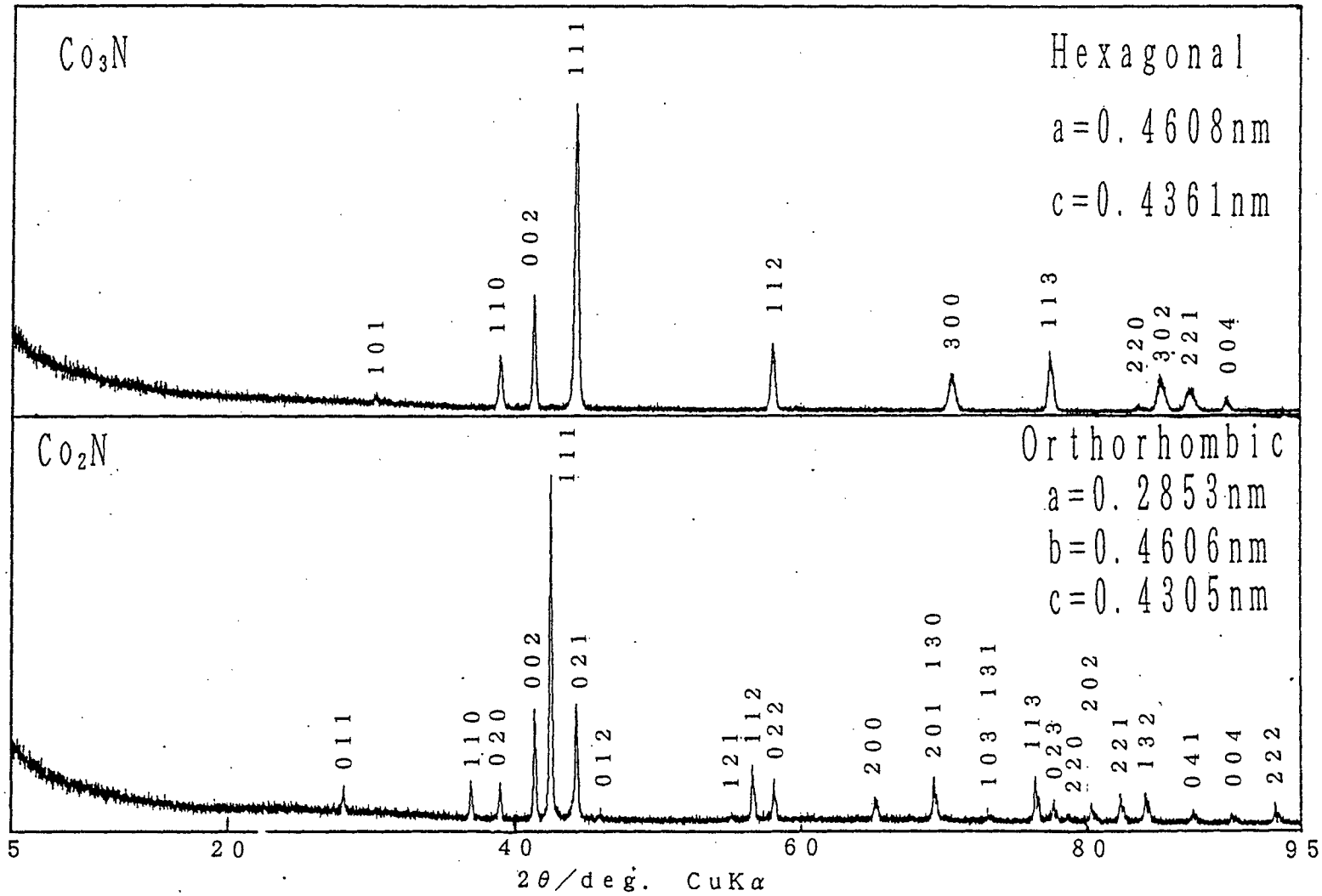


Fig. 1. X-ray diffraction patterns of $Co_3N$ and $Co_2N$.

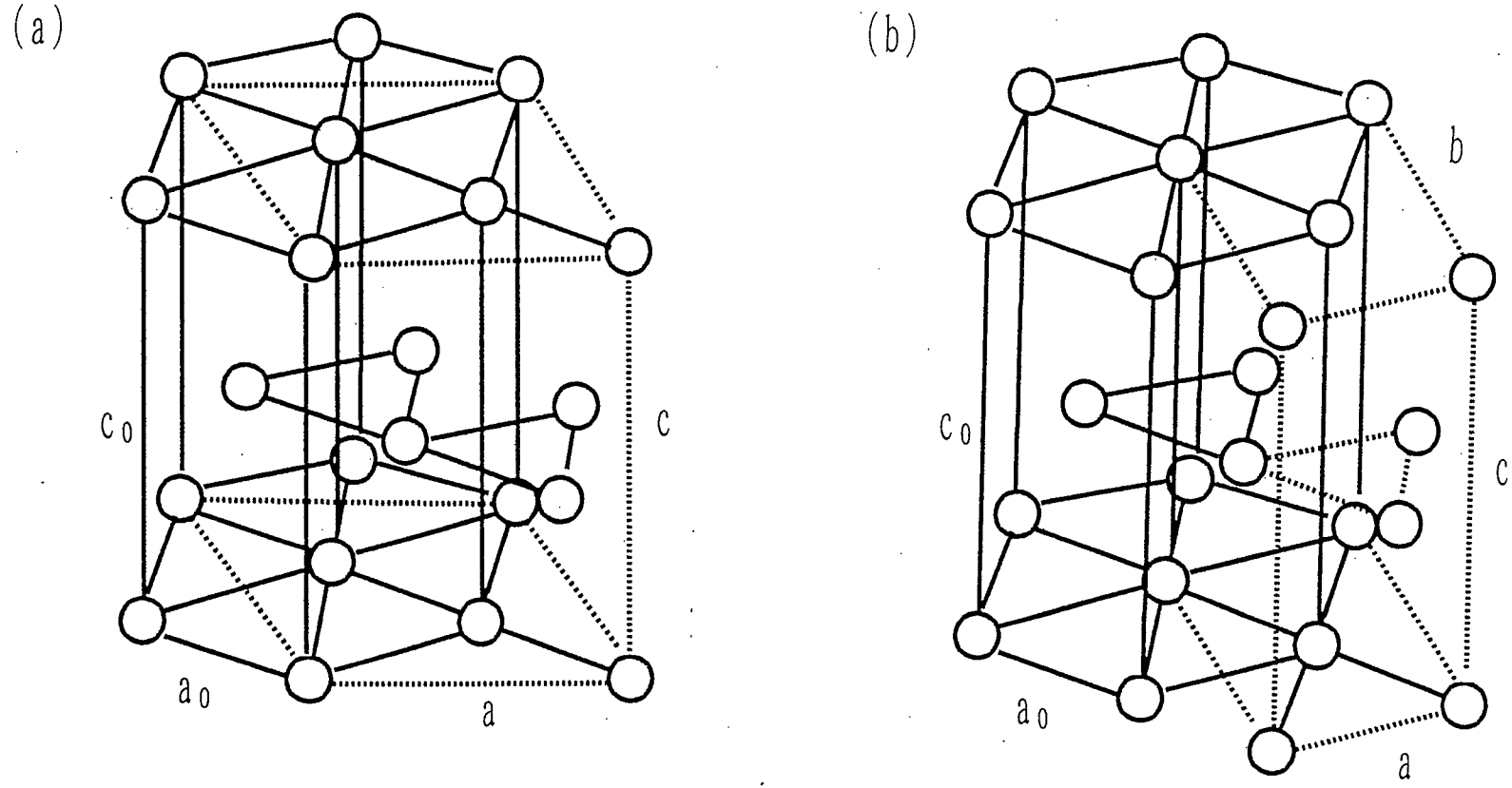


Fig. 2. Metal arrangements and unit cells of $Co_3N$ (a) and $Co_2N$ (b). Open circle denotes a Co atom. The unit cells of $Co_3N$ and $Co_2N$ are expressed by dotted lines. $a_0$ and $c_0$ correspond to the lattice parameters of $Co_3N$ and $Co_2N$. The relations between cell dimensions of them and hcp arrangement of Co atoms were as follows, $a=\sqrt{3}a_0$ and $c=c_0$ in $Co_3N$, and $a=a_0$, $b=\sqrt{3}a_0$ and $c=c_0$ in $Co_2N$, respectively.

Carbon and Chlorine impurities in $Co_3N$ and $Co_2N$ were not detected. The chemical composition for $Co_3N$ and $Co_2N$ were evaluated to be $Co_3N_{1.02}$-$Co_3N_{1.18}$ and $Co_2N_{0.98}$, respectively, by thermal conductivity method. The composition range for $Co_3N$ was close to the previous data of $Co_3N_{1.05}$-$Co_3N_{1.10}$ [3]. It was found that $Co_3N$ contained excess N atoms, but $Co_2N$ with N deficiency was close to stoichiometric.

Fig. 3 displays the XRD pattern of $Ni_3N$. This pattern was indexed by a hexagonal unit cell (a=0.8010nm, c=0.4309nm). However, the value of the a-parameter for $Ni_3N$ correspond to 3 times that for hcp arrangements of Ni atoms. This result is contrary to those of $Co_3N$, $Ni_3N$ and $Fe_{2-3}N$ [17]. The fact suggests that the arrangements of N atoms in $Ni_3N$ slightly differ from those in $Fe_{2-3}N$, $Ni_3N$ and $Co_3N$. The presence of C and Cl in $Ni_3N$ were also not observed. $Ni_3N$ possessed the N content corresponding to $Ni_3N_{1.00}$-$Ni_3N_{1.01}$. Consequently, $Ni_3N$ prepared by firing $NiCl_2$ in $NH_3$ flowing contains excess nitrogen but very close to stoichiometric.

### 3.2 *Magnetic properties of $Co_3N$, $Co_2N$ and $Ni_3N$*

Temperature dependence of magnetic susceptibility of $Co_3N$ and $Co_2N$ were shown in Fig. 4. Values of $\sigma_s$ at 293K for $Co_3N$ and $Co_2N$ were estimate to be 3.6±0.4Gcm$^3$/g and 0.23±0.05Gcm$^3$/g by extrapolating $\sigma$ to zero magnetic field in $\sigma$-$H$ curves, respectively. Amounts of α-Co impurity in $Co_3N$ and $Co_2N$ were in the order of 2.0-2.5wt% and 0.11-0.16wt%, respectively, on assuming that the ferromagnetic impurity was only α-Co ($\sigma_s$=161.85Gcm$^3$/g, $T_c$=1394K [21]). The magnetic susceptibilities of $Co_3N$ and $Co_2N$ were calculated after correcting the observed values of $\sigma$ with $\sigma_s$. Values of $\chi$ at room temperature for $Co_3N$ and $Co_2N$ were (20±4)×10$^{-6}$cm$^3$/g and (3.3±0.2)×10$^{-6}$cm$^3$/g, respectively. The higher value of $\chi$ for $Co_3N$ than that for $Co_2N$ were found. Fig. 4 shows that both $\chi$ for $Co_3N$ and $Co_2N$ increase with decreasing temperature down to 83K. It is suggested that both nitrides exhibit paramagnetic behavior above 83K. It

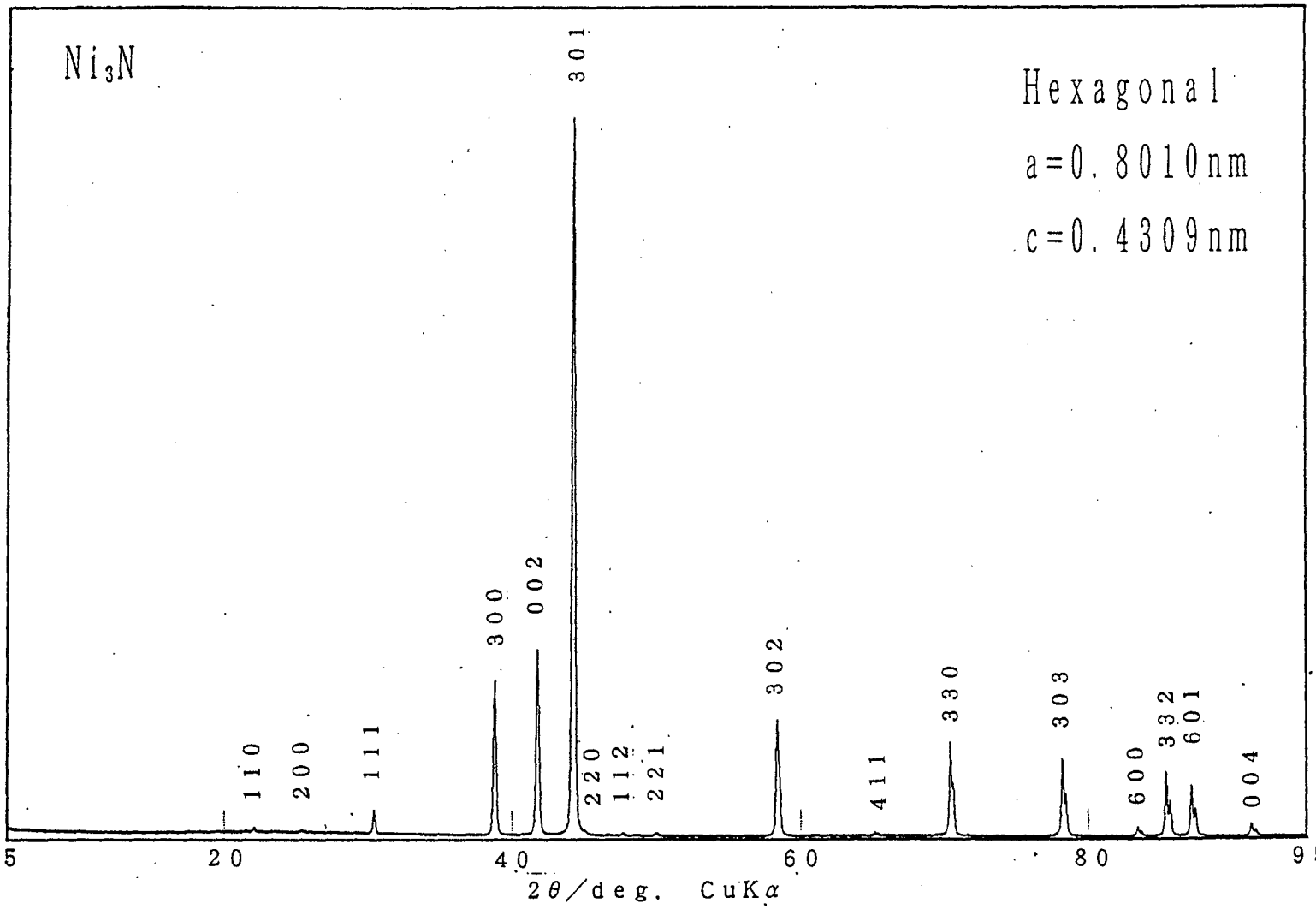


Fig. 3. X-ray diffraction pattern of $Ni_3N$.

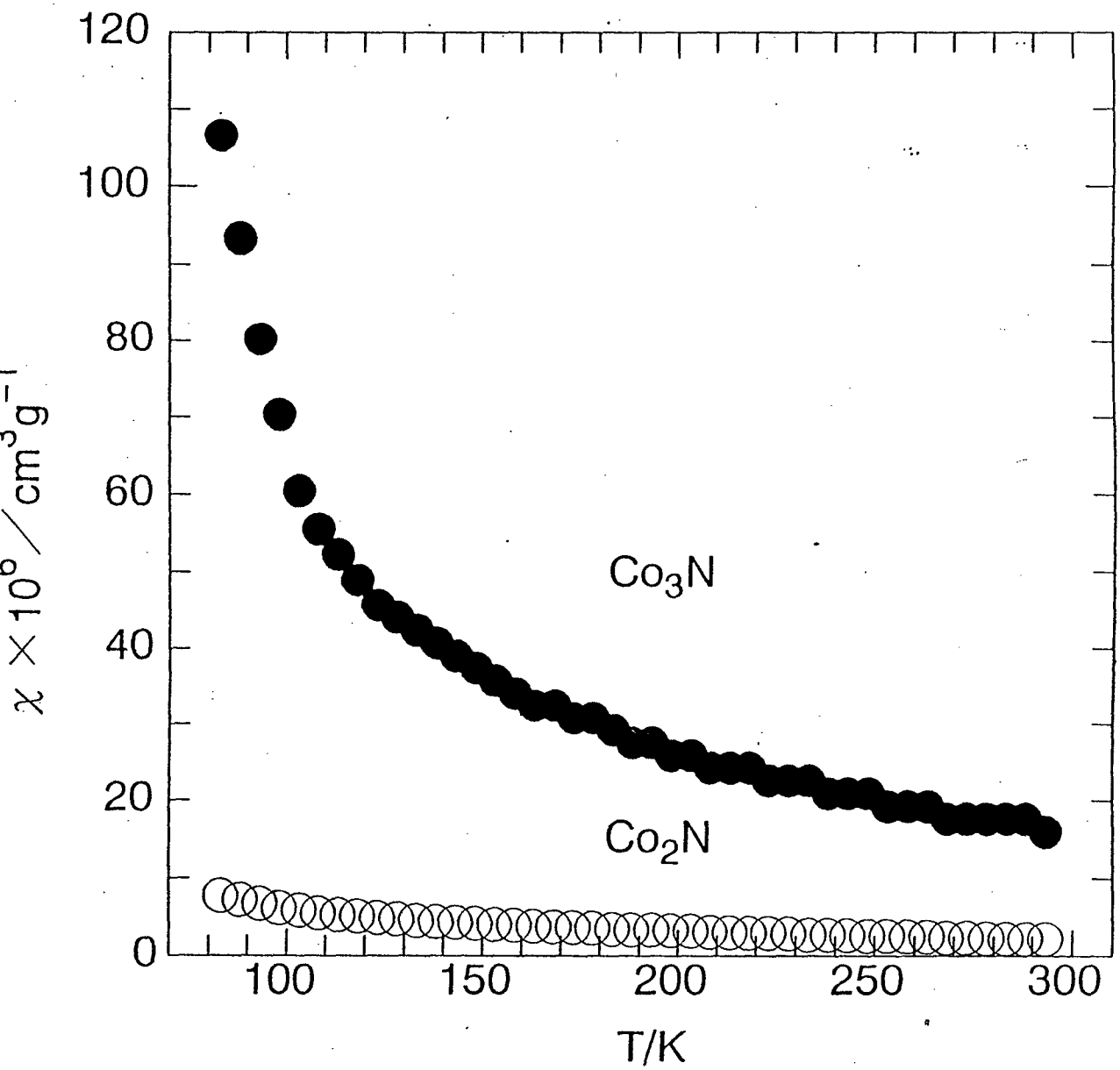


Fig. 4. Temperature dependence of magnetic susceptibility for $Co_3N$ and $Co_2N$.

is also found from Fig. 4 that the temperature dependence of $\chi$ for $Co_2N$ is smaller than that for $Co_3N$. Fig. 5 (a) and (b) depicts the temperature dependence of inverse molar susceptibilities $1/\chi_m$ for $Co_3N$ and $Co_2N$, respectively. On the basis of linear relationships between $1/\chi_m$ and $T$ for both $Co_3N$ and $Co_2N$, the magnetism for both compounds are found to be paramagnetism which follows Curie–Weiss law above 83K. The values of effective magnetic moments ($\mu_{eff}$) of $Co_3N$ and $Co_2N$ were calculated to be $1.4\pm0.1\mu_B$ and $0.65\pm0.5\mu_B$, respectively. The values are smaller than about $3\mu_B$ for $Fe_{2-3}N$ and $Fe_2N$ [19] and $3.15\mu_B$ for Co [22]. The values of the Weiss temperature ($\theta$) for $Co_3N$ and $Co_2N$ were +45±15K and −27±7K, respectively, as seen from Fig. 5. The ferromagnetic couplings in $Co_3N$ is expected below 60K. The Weiss temperature of $Co_2N$ is small and negative. It is presumed that the magnetic susceptibility is influenced by temperature independent paramagnetism such as Pauli paramagnetism or antiferromagnetic coupling takes place below 33K. The values of $\theta$ and $\mu_{eff}$ of Co nitride denoted as $Co_3N$ were reported to be −500K and $3\pm0.3\mu_B$. The difference in the magnetic properties between the present result and the previous data [9] for $Co_3N$ is attributed to a difference in chemical composition between them, i. e. real chemical composition is $Co_3N_{1.55}$.

Temperature dependence of magnetic susceptibility ($\chi$) and inverse molar susceptibility ($1/\chi_m$) for $Ni_3N$ were shown in Fig. 6 (a) and (b), respectively. The values of $\sigma_s$ at room temperature for $Ni_3N$ samples varied in the range between $3.2\times10^{-3}$ and $6.2\times10^{-3}Gcm^3/g$. Ni metal impurity in $Ni_3N$ was evaluated as less than 0.01wt%, on assuming that the ferromagnetic impurity in samples was only Ni ($\sigma_s$=55.01$Gcm^3/g$, $T_c$=631.0K [22]). The value of $\chi$ for $Ni_3N$ at room temperature was $(1.12\pm0.01)\times10^{-6}cm^3/g$ and which was fairly smaller than that for $Co_3N$. $\chi$ of $Ni_3N$ increases with decreasing temperature as seen in Fig. 6 (a). The linear relationship in the $1/\chi_m$–$T$ plot in Fig. 6 indicates that the magnetism of $Ni_3N$ is paramagnetic above 83K which obeyed

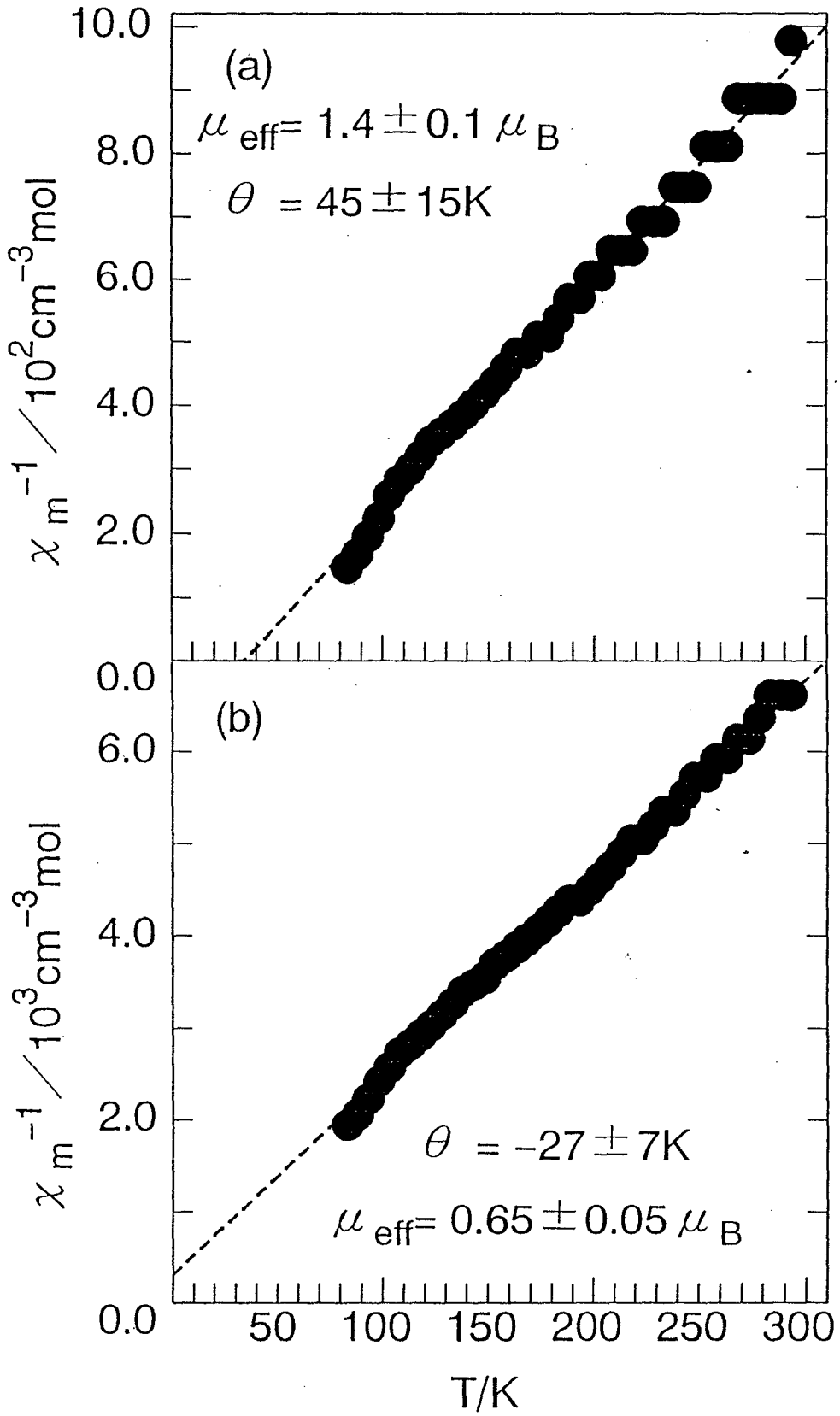


Fig. 5. Temperature dependence of inverse molar susceptibility for $Co_3N$ (a) and $Co_2N$ (b). Weiss temperature, θ and the effective magnetic moment per a metal atom, $\mu_{eff}$ were described in this figure.

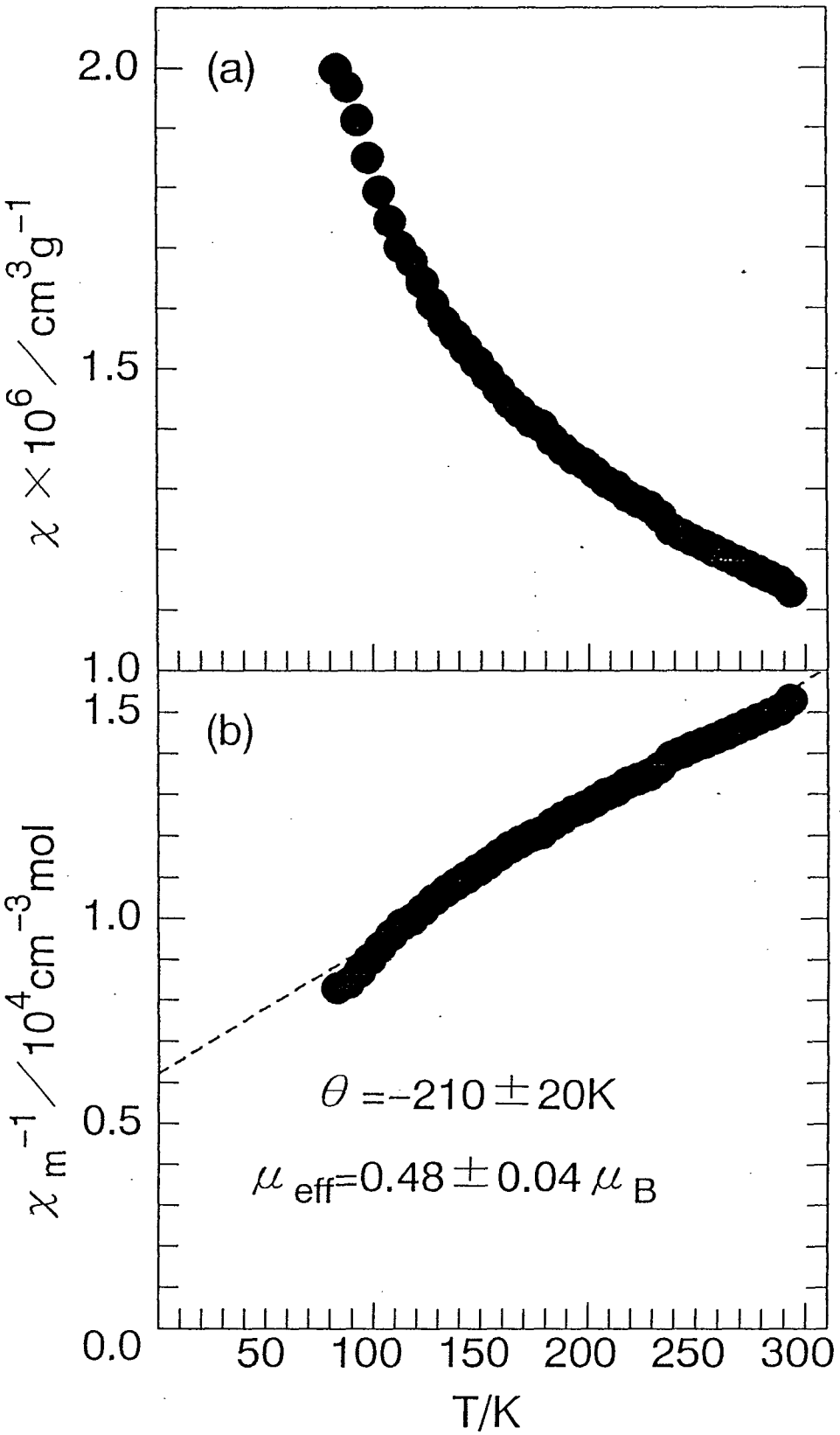


Fig. 6. Temperature dependence of magnetic susceptibility (a) and inverse molar susceptibility (b) for $Ni_3N$.

Curie–Weiss law. The values of $\mu_{eff}$ and θ for $Ni_3N$ were $0.48\pm0.04\mu_B$ and $-210\pm20$K, respectively, depending on the nitrogen content. The value of $\mu_{eff}$ for $Ni_3N$ is very small compared with $1.61\mu_B$ for Ni [22]. The Values of $\mu_{eff}$ for $M_3N$ (M=Fe, Co, Ni) decrease in order of $Fe_{2-3}N$, $Co_3N$ and $Ni_3N$. This tendency is analogous to that for their mother metals, where the $\mu_{eff}$ decrease with increasing number of valence electrons per a metal atom (*e/a*).

3.3 *Consideration in terms of magnetic properties of $M_{2-3}N$ and $M_2N$*

The magnetisms of most of $M_{2-3}N$ and $M_2N$ are usually discussed in connection with those of their mother metals [19] and alloys. In general, magnetic susceptibility of a transition metal consists of the terms of Larmor diamagnetism ($\chi_d$), temperature dependent paramagnetism ($\chi_c$) and temperature independent paramagnetism ($\chi_{PL}$) as follows [23],

$$\chi = \chi_d + \chi_c + \chi_{PL} \qquad (1).$$

$\chi_d$ of a compound is equal to the sum of diamagnetic susceptibilities of constituent atoms. The values of $\chi_d$ for $M_3N$ were calculated to be $(-2.5\pm0.5)\times10^{-5}$cm$^3$/mol by the sum of $\chi_m$ of M and N atoms. The value of $\chi_d$ is smaller by one or two orders than those of $\chi$ for $M_3N$. $\chi_c$ is the temperature dependent term which obeys Curie–Weiss law as follows [23],

$$\chi_c = \frac{N\mu_{eff}^2}{3k}\frac{1}{T-\theta} \qquad (2).$$

Where $k$, θ and $N$ are Boltzmann constant, Weiss temperature and Avogadro number, respectively.

$\chi_{PL}$ corresponds to the terms of sum of Pauli paramagnetism and Landau diamagnetism. The relation between $\chi_{PL}$ and the density of state at Fermi level $D(E_F)$ holds as follows [22],

$$\chi_{PL} = \frac{2}{3} D(E_F)\mu_B^2 \qquad (3).$$

Where $\mu_B$ is Bohr magneton. Since $\chi_{PL}$ is independent on temperatures, the contribution of $\chi_{PL}$ to $\chi$ becomes large at high temperature. The values of $\chi_{PL}$ obtained by subtracting the $\chi_d$ and $\chi_c$ from $\chi$, are $(3.1\pm0.8)\times10^{-4}$cm$^3$/mol for $Co_3N$ and $(8.2\pm0.7)\times10^{-5}$cm$^3$/mol for $Ni_3N$, respectively. The decrease in the values of $\chi_{PL}$ from $Co_3N$ to $Ni_3N$ can be understood by relating to the decrease in $D(E_F)$ with increasing 3d electrons in their 3d bands.

It was considered that the magnetic properties of these nitrides are mainly contributed with the 3d bands consist of metal valence electrons. Therefore, the values of $\mu_{eff}$ were plotted against valence electrons per a metal atom, *e/a* of $Mn_2N$ [24], $Fe_{2-3}N$ [19], $Fe_2N$ [19], $Co_3N$, $Co_2N$ and $Ni_3N$ in Fig. 7. It were worth noting that the overall feature in the $\mu_{eff}$–*e/a* relations for $M_{2-3}N$ and $M_2N$ lines is similar to those for 3d transition metal alloys [25]. This fact supported also experimentally the large contribution of 3d bands to the magnetic properties for $M_{2-3}N$ and $M_2N$. This behavior, which magnetic moments per a metal atom ($\mu_M$) and $\mu_{eff}$ varied with *e/a* like Slater–Pauling curve as shown in Fig. 8, were observed in 3d transition metal phosphide, $M_3P$ [26] and boride, $M_2B$ and MB [27].

$Co_3N$, $Co_2N$ and $Ni_3N$ possessed considerably lower $\mu_{eff}$ and magnetic transition temperatures compared to those of their mother metals and that the value of $\mu_{eff}$ for $Co_2N$ was smaller that for $Co_3N$ as mentioned previously. The effect of N atom on magnetic moment of metal nitride was also observed in the Fe and N system, in which $\mu_{Fe}$ and $T_c$ decreased with an increase of nitrogen content [19, 28].

Mekata *et al.* attributed the difference in the magnetic properties between $Fe_{2-3}N$ and $Fe_2N$ to the difference of environment around a metal site between them [19]. The difference of the magnetic properties between $Co_2N$ and $Co_3N$ may be understood on the

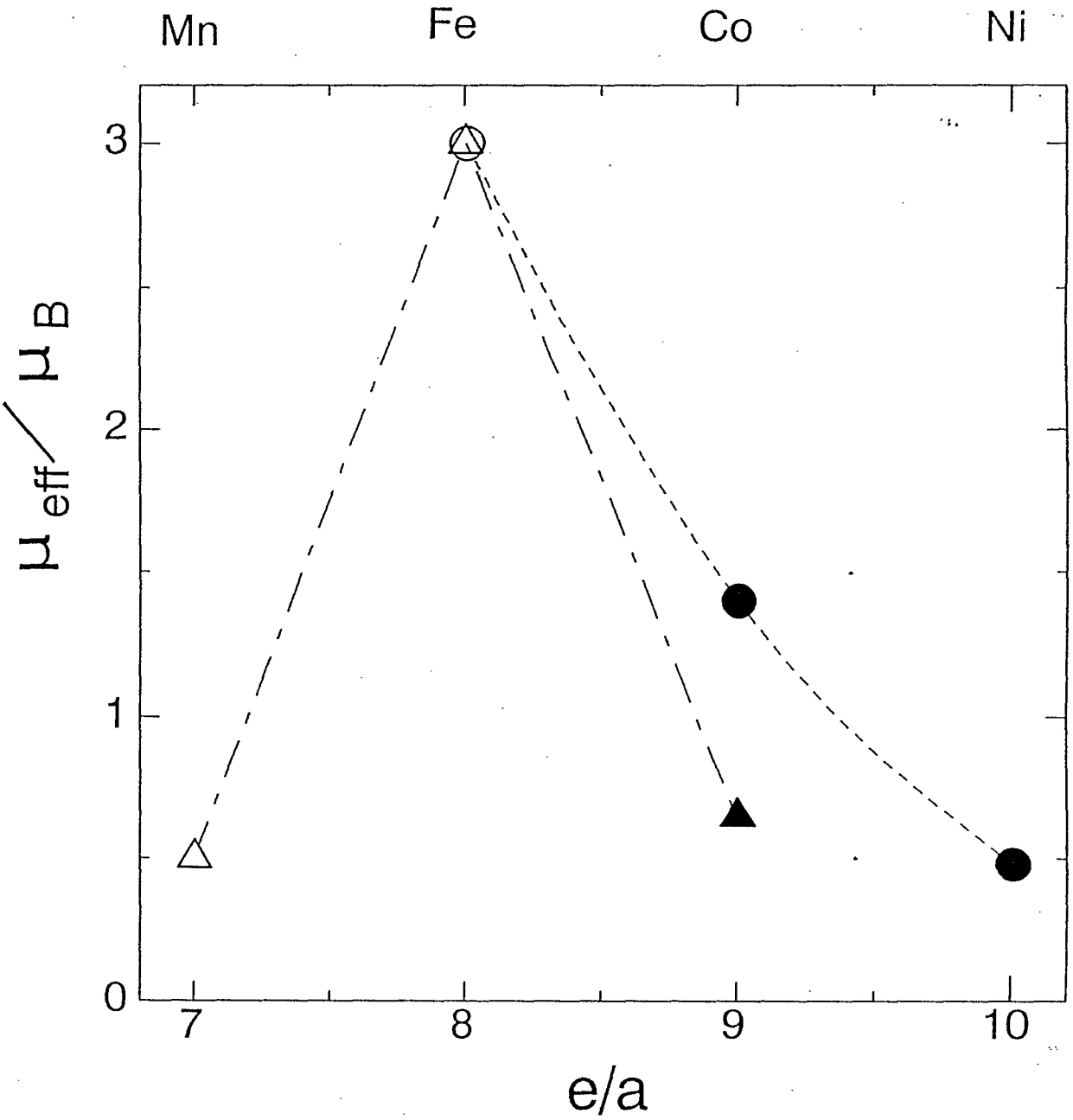


Fig. 7. The relation between the formal valence electron number per a metal atom, *e/a* and the effective magnetic moment per a metal atom, $\mu_{eff}$ for $M_{2-3}N$ (○ [19], ●; present results) and $M_2N$ (△ [19], ▲; present results). Dot-dashed line and dotted curves show that $\mu_{eff}$ of $M_2N$ and $M_{2-3}N$, respectively, exhibit the behavior such as Slater-Pauling curve observed in 3d metal alloys.

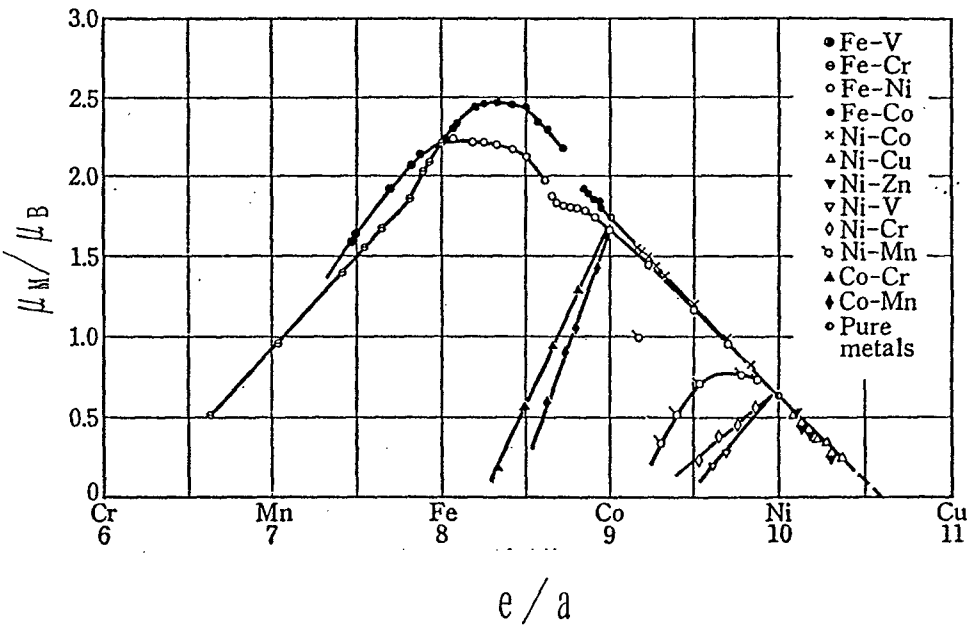


Fig. 8. The relation between magnetic moment per a metal atom ($\mu_M$) and number of valence electrons per a M atom ($e/a$) in 3d metals and their alloys "Slater–Pauling curves" [22].

viewpoint of N-coordination number around a M atom. Fig. 9 depicts the types of environments around a metal site in $M_3N$ and $M_2N$. A metal atom occupies at the body center of trigonal prism consist of octahedral interstitial sites which are partially occupied by N atoms. Since N atoms in $M_3N$ and $M_2N$ are surrounded by six metal atoms, one of the type of environment in Fig. 9 (a) is dominant at the composition near to $M_3N$ and the other type in Fig. 9 (b) present primarily at the composition close to $M_2N$. Mössba uer spectrum for $Fe_{2.5}N$ confirmed the presence of Fe atoms with two different internal fields [19], indicating that Fe atoms in $Fe_{2.5}N$ possess different magnetic moments which reflect the environments around a Fe atom. On the basis of the values of magnetization and internal field for $Fe_{3.2}N$, $Fe_{2-3}N$ and $Fe_2N$ [18, 19, 28, 29], the values of $\mu_{Fe}$ of Fe atoms with two and three neighboring N atoms were evaluated to be 1.9–2.0$\mu_B$ and 0.12–0.19$\mu_B$, respectively. It is thought that the difference in $\mu_{eff}$ for $Co_3N$ and $Co_2N$ is analogous to the variation of magnetic moment in $FeN_y$ described above, i.e. $Co_3N$ possesses larger $\mu_{Co}$ compared with $Co_2N$, since $Co_3N$ surpasses $Co_2N$ with regard to the proportions of a Co atom with two neighboring N atoms.

## 4 *Summary*

Magnetic properties of $M_{2-3}N$ and $M_2N$ were studied to elucidate the effect of the kind of M and N-coordination number around a M atom on their effective magnetic moment.

$Co_3N$, $Co_2N$ and $Ni_3N$ were prepared by the thermal decompositions of $CoCl_2$ and $NiCl_2$ in $NH_3$ flow, were investigated to clarify through the measurements of magnetic susceptibilities in the temperature region between 83 and 293K. All of $Co_3N$, $Co_2N$ and $Ni_3N$ exhibit paramagnetism which obeyed Curie-Weiss law above 83K. The Values of effective magnetic moments for $Co_3N$, $Co_2N$ and $Ni_3N$ are estimated to be 1.4±0.1, 0.65±0.05 and 0.48±0.04$\mu_B$, respectively. In the system of $M_2N$ (M=Mn, Fe, Co), the

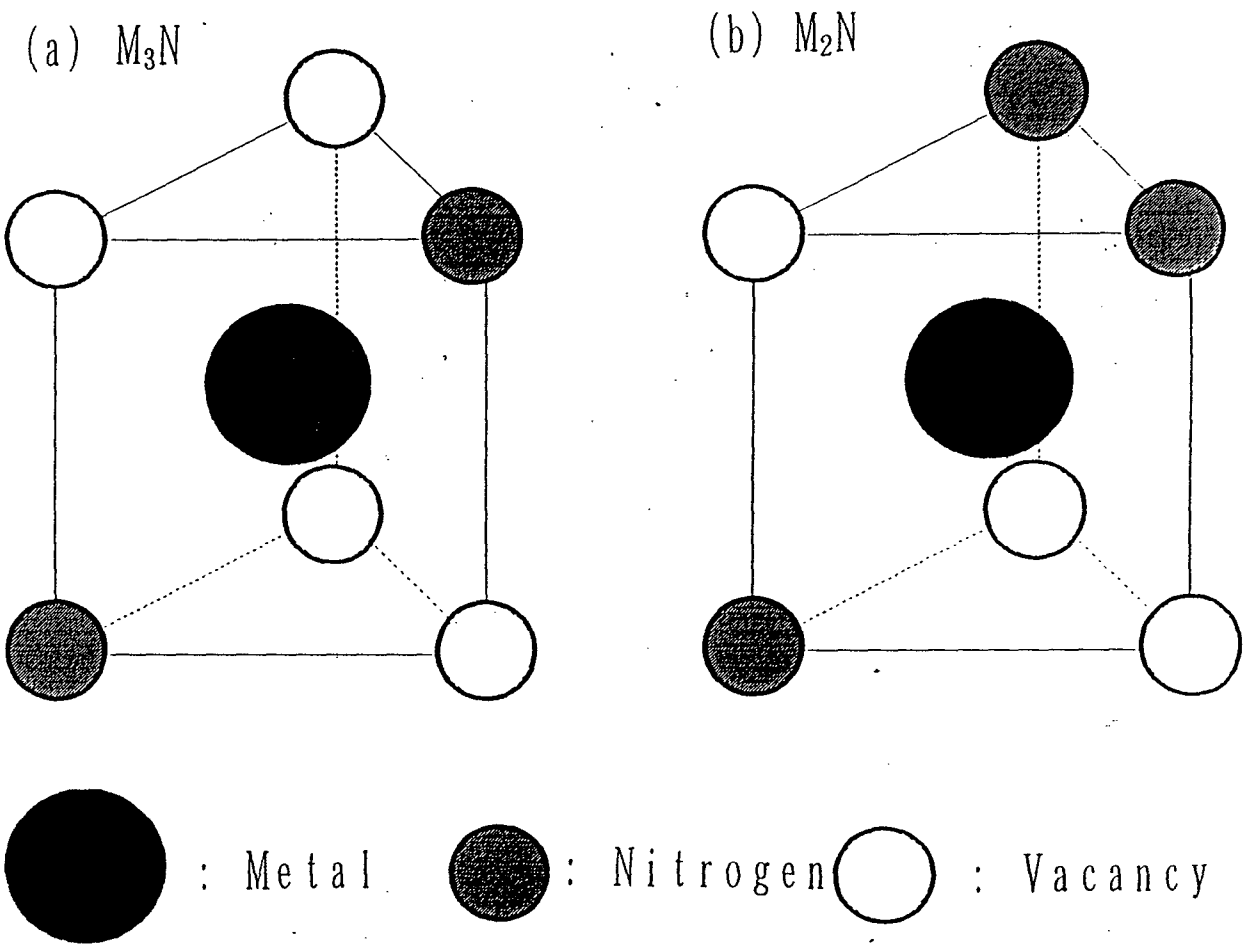


Fig. 9. Two types of environments around a metal site in $M_3N$ (a) and $M_2N$ (b).

effective magnetic moments were observed to be varied with the number of valence electrons of the M atom. In the system of $M_{2-3}N$, (M=Fe, Co, Ni), the effective magnetic moments, decreased monotonously with increasing the number of valence electrons of the M atom. It was found that these tendency of the relations between the effective moments and the number of valence electrons per a M atom for $M_2N$ and $M_3N$ are similar to those for 3d metals and their alloys whose the effective magnetic moments vary with the number of valence electrons of a 3d metals like "Slater–Pauling curves".

The difference in the effective magnetic moments between $Co_3N$ and $Co_2N$ may be related to that in N–coordination numbers around the Co atom between them, i.e. $\mu_{eff}$ of $Co_3N$ with the two nitrogen atoms adjacent to the Co atom is larger than that of $Co_2N$ with three nitrogen atoms adjacent to the Co atom. This result is consistent with the tendency observed at $MnN_y$ described in chapter 2.

*References*


1 N Terao, *Mem. Sci. Rev. Met., 57* (1960) 96.

2 K. Oda, T. Yoshio and K. Oda, *J. Mater. Sci., 22* (1987) 2729.

3 R. Juza and W Satze, *Z. Anorg. Chem., 253* (1945) 95.

4 O. Schmitz-Dumont, *Angew. Chem., 67* (1955) 231.

5 T. B. Joyner and F. H. Verhoek, *J, Am. Chem. Soc. 83* (1961) 1070.

6 M. Manzel, E. Steinbeiss and W. Schüppel, *Phys. Status Solidi (a) 119* (1990) 279.

7 M. Matsuoka, K. Ono and T. Inukai, *IEEE Trans Magn., 23 [5]* (1987) 2788.

8 M. Matsuoka, K. Ono and T. Inukai, *Appl. Phys. Lett., 49* (1986) 977.

9 K. H. Mader, F. Thieme and A. Knappwost, *Z. Anorg. Allg. Chem. 366* (1969) 274.

10 G. J. W. R. Dorman and M. Sikkens, *Thin Solid Films, 105* (1983) 251.

11 N. Terao and A. Berghezan, *J. Phys. Soc. Jpn., 14 [2]* (1959) 139.

12 N. Terao, *J. Phys. Soc. Jpn., 15 [2]* (1960) 227.

13 H. A. Wriedt, *Bull. Alloy Phase Diagrams, 6 [6]* (1985) 558.

14 G. W. Watt and D. D. Davis, *J. Am. Chem. Soc. 70* (1948) 3753.

15 A. Benardoum, F. Rémy and J. Bernard, *C. R. Acad. Sci. (Paris) 266* (1968) 1579.

16 L. Reimer, *Z. Phys., 149* (1957) 425.

17 R. Juza, *Adv. Inorg. Chem. Radiochem. 9* (1966) 81.

18 J. B. Goodenough, A. Wold and R. J. Arnott, *J. Appl. Phys., 31 [5]* (1960) 342S.

19 M. Mekata, H. Yoshimura and H. Takaki, *J. Phys. Soc. Jpn., 33* (1972) 62.

20 J. Clarke and K. H. Jack, *Chem. Ind. (London), 1951* (1951) 1004.

21 H. P. Meyers and W. Sucksmith, *Proc. Roy. Soc. A 207* (1951) 427.

22 S. Chikazumi, K. Ohta, K. Adachi, N. Tsuda and Y. Ishikawa (eds.), *Jiseitai handbook,* Asakura-Shoten (1975).

23 Nippon Kagakukai (eds.), *Kagakubinran Kisohen* II, 3rd Ed., Maruzen, (1984) pp. 510.

24 M. Mekata, J. Haruna and H Takaki, *J. Phys. Soc. Jpn. 25* (1968) 234.

25 Y. Kakehashi, *Prog. Thor. Phys. Suppl., 101* (1990) 105.

26 R. J. Gambino, T. R. McGuire and Y. Nakamura, *J. Appl. Phys., 38* (1967) 1253.

27 M. C. Cadeville and A. J. P. Meyer, *Compt. Rend. 255* (1962) 3391.

28 A. Wold, R. J. Arnott and N. Menyuk, *J. Phys. Chem., 65* (1961) 1068.

29 K. H. Eickel and W. Pitsch, *Phys. Status Solidi, 39* (1970) 121.

## Chapter 5 Preparation and their electric properties of manganese nitride $MnN_y$ ($0<y<1$) thin films by reactive vapor deposition method

### 1. *Introduction*

Manganese nitrides ($MnN_y$) ($0<y<1$) have been reported to take four crystal phases, $Mn_4N$, $Mn_{2-3}N$, $Mn_3N_2$ and $Mn_6N_5$ so far. The powders and single crystals of $MnN_y$ were prepared by nitrizing manganese amalgams [1], the thermal decomposition of $Na_2[Mn(NH_2)_4]$ [2] and the reaction between $MnI_2$ and $NaNH_2$ in high $NH_3$ pressure [2]. $Mn_4N$ and $Mn_6N_5$ films were obtained by reaction of α–Mn film with $NH_3$ gas at 573K [3, 4]. The magnetic properties of $Mn_4N$ [5, 6] and $Mn_{2-3}N$ [7, 8] with the crystal structures analogous to $Fe_4N$ and $Fe_{2-3}N$, respectively, were clarified previously. The antiferromagnetic structure of $Mn_3N_2$ was determined by the measurement of unpolarized neutron diffraction at 11 and 291K [2]. There are many reports on electrical resistivity of TiN film [9], CrN film [10] $Fe_4N$ sheet [11] and $Ni_3N$ powder [12]. However, electrical resistivity of $MnN_y$ have scarcely been investigated, except a report describing that $Mn_3N_2$ exhibits a metallic conductivity [13]. The serious problem on preparation of Mn nitrides is coexistence of manganese oxides as a by–product which hamperes characterization of Mn nitrides.

In this work, $MnN_y$ films were prepared by reactive vapor deposition method. Since this vapor deposition process is distinct in the point of reaction temperature from the direct nitrization process of Mn powder with $NH_3$ or $N_2$ flowing, this process can be expected for the formation of $MnN_y$ with large nonstoichiometry of nitrogen and also for elimination of by products such as MnO. The electrical properties of $MnN_y$ films were clarified by measurement of electrical resistivity of the Mn oxides free samples.

2. *Experimental*

Fig. 1 shows the schematic drawing of the apparatus used for preparation $MnN_y$ films. The reaction chamber was made of pyrex glass. The reaction chamber consists of two gas inlets, a W filament for vaporizing Mn metal and electrodes for glow discharge, which is made of W rods and Ta plates. $N_2$ gas (99.9999% in purity, Osaka Sanso Kogyo Co.) and α–Mn flakes (99.9% in purity, Nakalai Tesque Co.) were used as the source of the reaction. The reaction chamber were evacuated down to a pressure of $\leq 6.5\times10^{-3}$Pa by oil rotary pump and oil diffusion pump through a liquid nitrogen trap. The α–Mn flakes placed on the W filament were preheated under vacum of 0.13Pa to remove the contamination such as oxigen and water on their surface with closing the shutter. After the reaction chamber was evacuated again down to $6.5\times10^{-3}$Pa, nitrogen gas flow into the chamber was initiated and then nitrogen gas pressures was kept constant at desired one by regulating the leak valve (LV in Fig, 1). Nitrogen gas was activated by the glow discharge induced by high voltage of 10kV. Then the shutter was opened and α–Mn was vaporized by applying electric power to the W filament. The electric power ($E_p$) between 100 and 300W was regulated in order to control nitrogen content of products. The deposition time of film was varied from 5 to 30 min. The bright emission like plasma was observed during the deposition. Slide glasses or polystyrene coated slide glasses were used for the substrates. A Chromel–Alumel thermocouple was put over the substrate. No efforts were made to heat substrates. The substrate temperature during the deposition was in the range between 373 and 523K. The nitrogen gas pressure ($p_N$) during the deposition was set at desired pressures between 1.3 and 26Pa and the fluctuation of $p_N$ was depressed within ±0.65Pa. The thickness of the films ranged from 0.2 to 0.8μm. The powder samples were obtained by dissolving the polystyrene films between the deposited film and the substrate in tetrahydrofuran.

The crystalline phase in both the deposited films and the powders was identified

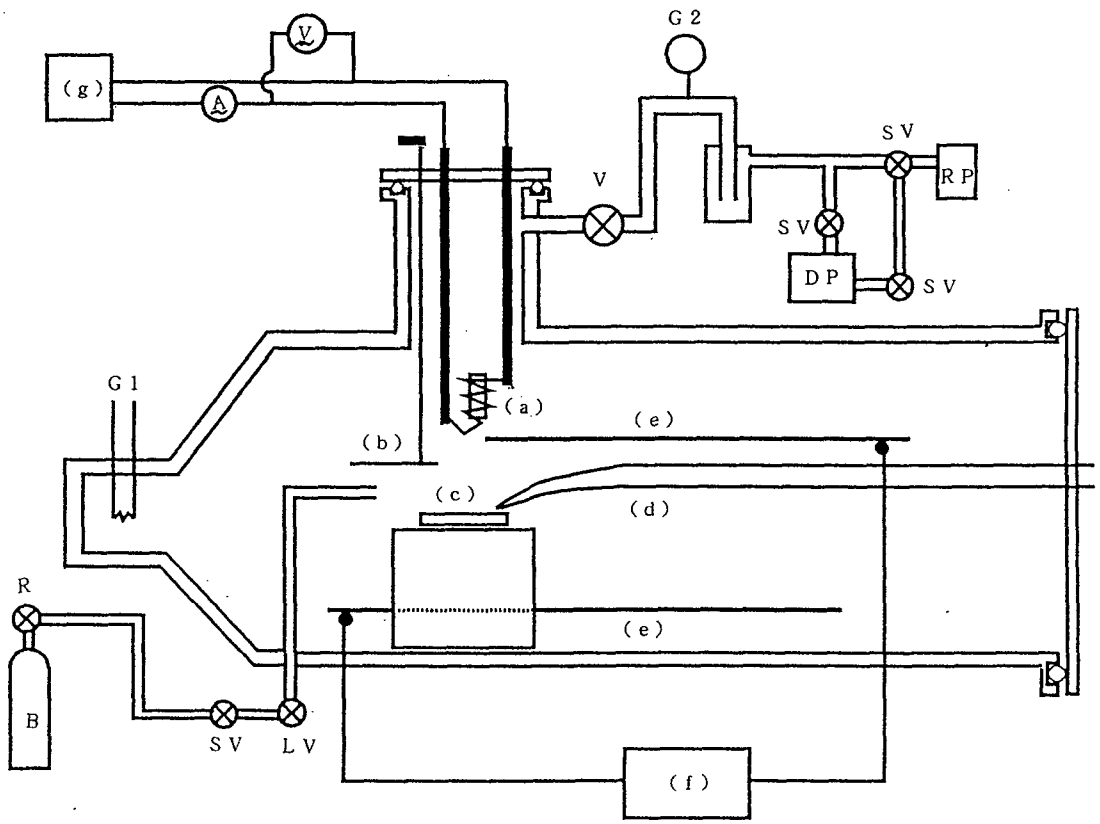


Fig. 1 Schematic drawing of the apparatus used for the reactive vapor deposition. (a); W filament where α–Mn flakes are placed, (b); shutter, (c); substrate, (d); thermocouple, (e); Ta electrode for glow discharge, (f); neon transformer, (g); electric power supply, A; ammeter, V; voltmeter, G1; pirani gauge, G2; ionization gauge, LV; leak valve, SV; stop valve, R; regulator for $N_2$ gas cylinder, V; main valve, and conductance valve, DP; oil diffusion pump, RP; rotary pump.

using a X-ray diffractmeter (CuKα radiation, Rotaflex/RINT, Rigaku Co.). The lattice parameters of powder samples were determined from X-ray diffraction (XRD) measurement by using silicon as an internal standard. The nitrogen content in the powder samples was determined by CHN analysis using 240C, Perkin Elmer Co. The electrical resistivity of deposited films was measured by four point probe method in the temperature range between 5 and 295K, and film thickness was measured with using nanoscope (Model 911-9150, Anelva Co.).

## 3. *Results and discussion*

### 3.1 *Structure and composition of the deposited films*

The crystalline phase in the films varied with depending on deposition parameters, $E_p$ and $p_N$. The films contained both phases of α-Mn and $Mn_4N$ only when depositing the films without glow discharge and the bright emission. Figs. 2, 3 and 4 show XRD patterns of the films deposited at various conditions comparing with those of $Mn_6N_5$, $Mn_3N_2$ and $Mn_4N$ obtained by heating α-Mn powder in $N_2$ or $NH_3$ flow, respectively. In all XRD patterns of the films, no peaks of Mn oxides were detected. $Mn_{2-3}N$ with hexagonal lattice has not been obtained in the present work. The XRD patterns of $Mn_3N_2$ and $Mn_6N_{6.42}$ films exhibit a strong preferred orientation with the closest packing plane of Mn atoms parallel to the substrate, but the powder samples of $Mn_3N_2$ and $Mn_6N_{6.42}$, which were obtained by tearing off the films from the substrates, showed the same XRD patterns to those of $Mn_3N_2$ and $Mn_6N_5$, respectively. The XRD patterns of the $Mn_4N$ films agrees with that of $Mn_4N$, but no preferred orientation is observed as shown in Fig. 2. The width of XRD peaks of the $Mn_4N$ film were broader than those of the $Mn_6N_5$ and $Mn_3N_2$ films, in spite of the no difference in film thickness among them. These results imply that the crystallinity of the $Mn_4N$ film is poorer than those of the others. The $Mn_4N$ film was obtained only in the case when glow discharge was blinking because of low $E_p$ and

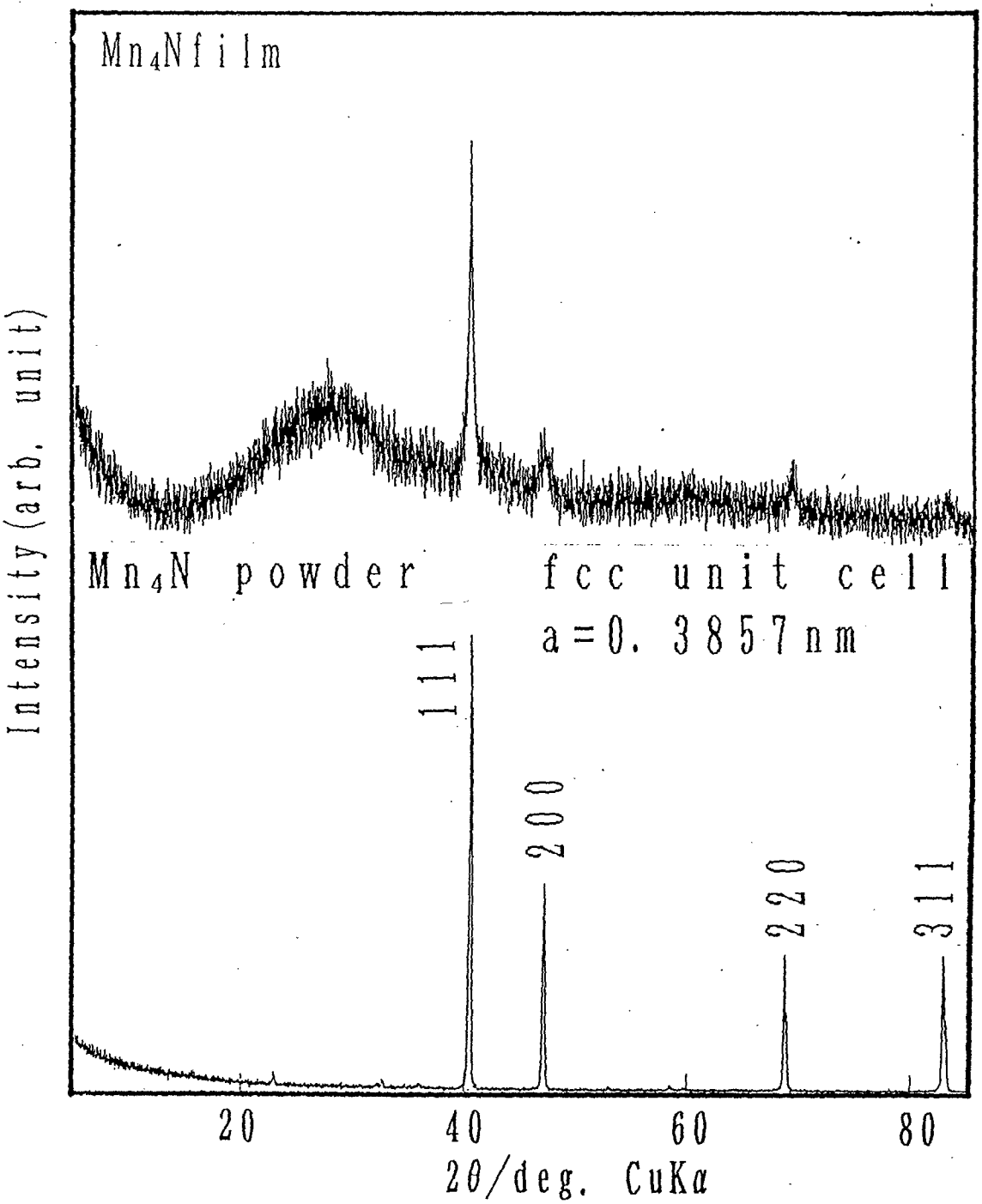


Fig. 2 X-ray diffraction patterns for the $Mn_4N$ film deposited at $E_p$ of 155W and $p_N$ of 1.3Pa, and $Mn_4N$ powder obtained successively firing α-Mn powder at 1073K in $N_2$ and $H_2$ flow.

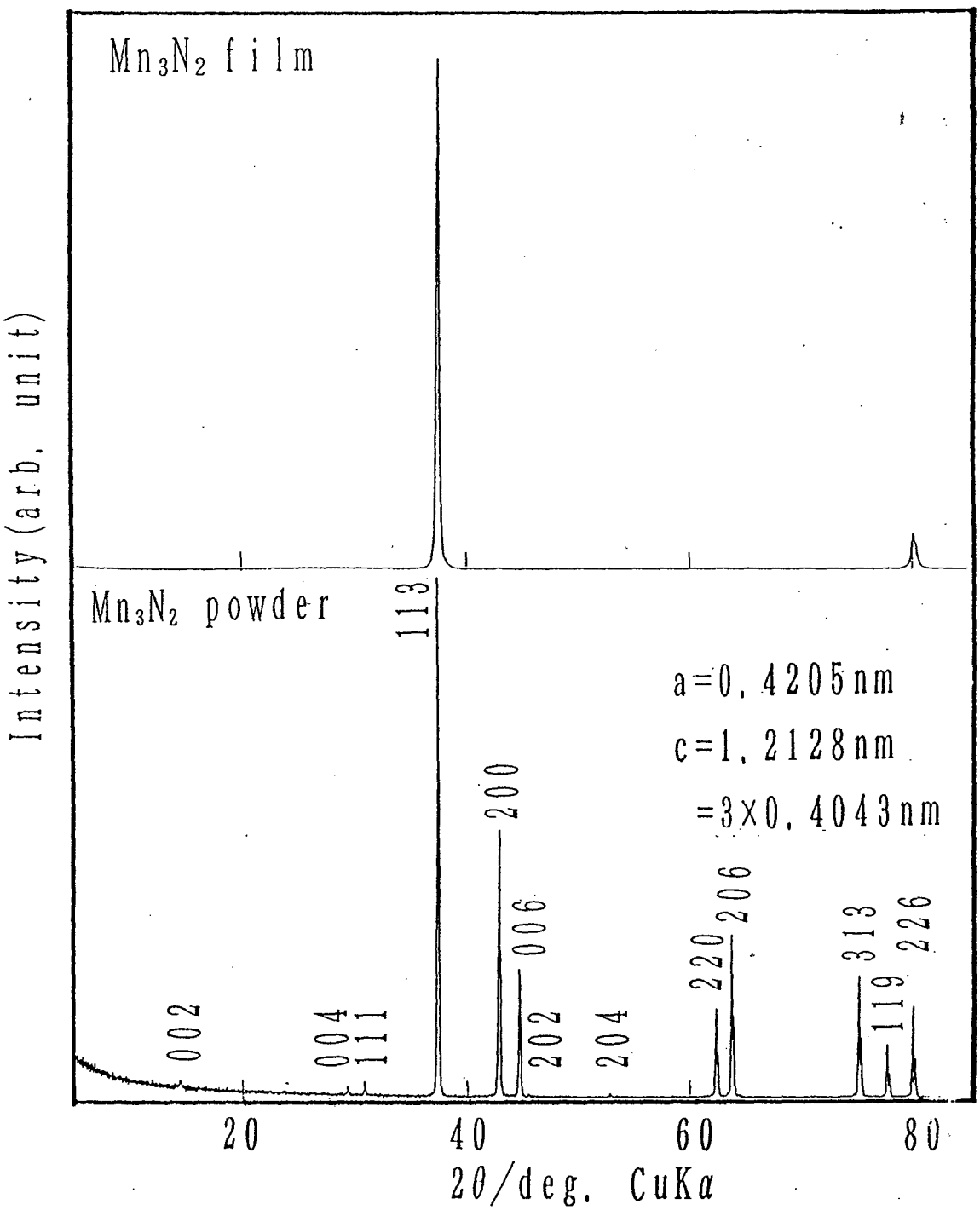


Fig. 3 X-ray diffraction patterns for the $Mn_3N_2$ film deposited at $E_p$ of 240W and $p_N$ of 2.6Pa and $Mn_3N_2$ powder obtained successively firing α-Mn powder at 873K in $NH_3$ and $H_2$ flow.

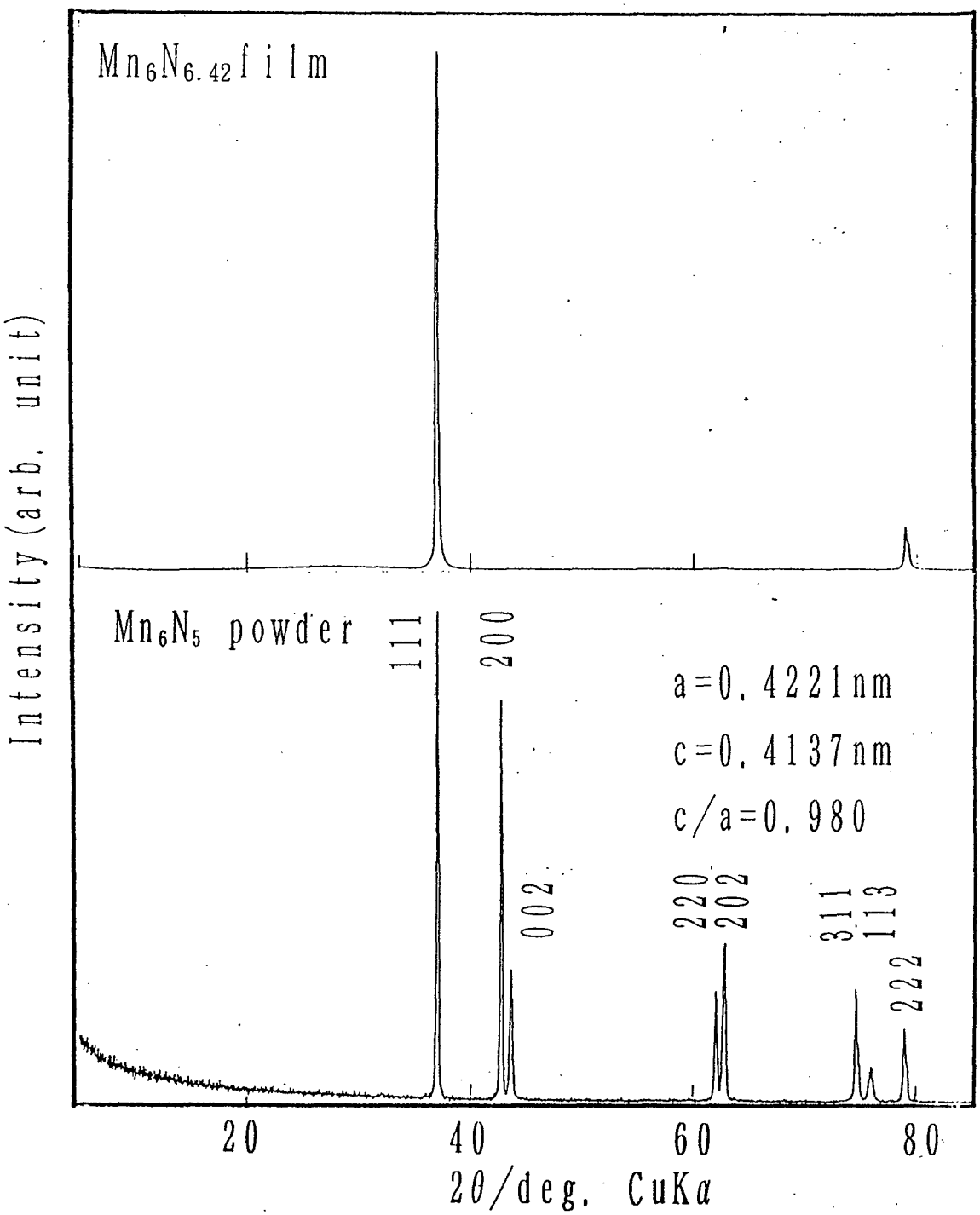


Fig. 4 X-ray diffraction patterns for the $Mn_6N_{6.42}$ film deposited at $E_p$ of 186W and $p_N$ of 25Pa and (b) $Mn_6N_5$ powder obtained firing α-Mn powder at 873K in $NH_3$ flow.

low $P_N$. Such the fact suggests that the stability of the glow discharge during the deposition affects micro structure of the films.

Deposition conditions, nitrogen contents and lattice parameters for the $MnN_y$ films are listed in Table 1. Values of the lattice parameters of $Mn_3N_2$, $Mn_4N$ and $Mn_6N_5$ films are consistent with previous reported data [1], respectively, as shown in Table 1. One third of the c axis of $Mn_3N_2$ is also shown in parentheses. As seen in Fig. 5. the XRD pattern of $MnN_{0.64}$ powder, which was obtained by tearing off the films from the substrates, is different from that of $Mn_3N_2$ but the pattern is similar to that of $Mn_6N_5$ with no superlattice diffractions which are observed of $Mn_3N_2$ with an ordered arrangement of nitrogen atoms. Furthermore, it is found that values of lattice parameters of $MnN_{0.64}$ and $MnN_{0.71}$ films were comparable to those of $Mn_6N_5$ reported previously [1] rather than the value of c/3 of the $Mn_3N_2$, in spite of their nitrogen contents close to that of $Mn_3N_2$. Though $Mn_6N_5$ and $Mn_3N_2$ have the fct lattice (c/a<1) of Mn atoms, it was pointed out that they differ in the arrangement of nitrogen atoms [2, 4, 13] each other. Nitrogen vacancies at octahedral site in $Mn_3N_2$ arrange regularly to result in the c axis of 3×c (primitive fct lattice of Mn), while those in $Mn_6N_5$ were presumed to distribute randomly [2, 4, 13]. Because of the ordering of nitrogen vacancies in $Mn_3N_2$, the value of c/3 of $Mn_3N_2$ is smaller, compared to the c axis of $Mn_6N_5$. Thus, the $MnN_{0.64}$ and the $MnN_{0.71}$ films can be thought to be $Mn_6N_5$-type compounds. In the subsequent descriptions, that $MnN_{1.07}$ and $MnN_{1.08}$ films are called $Mn_6N_{5+\delta}$ film and $MnN_{0.64}$ and $MnN_{0.71}$ films are referred to as $Mn_6N_{5-\delta}$ film. The $Mn_6N_5$-type compound has been reported to be stable in a composition range between $MnN_{0.84}$ and the composition range $MnN_{0.95}$ at 573K and becomes narrow with increasing temperature [14]. The X-ray data on $MnN_{0.64}$, $MnN_{0.71}$, $MnN_{1.07}$ and $MnN_{1.08}$ films indicate that the composition range for $Mn_6N_5$-type compound is much wider than that reported previously. One of the reasons for existence of the large nonstoichiometry of $Mn_6N_5$ may be attributed to low deposition temperature.

Table 1 Deposition conditions, nitrogen contents and lattice parameters for $MnN_y$ films.

| Phase | $E_p$/W | $p_N$/Pa | $y$ in $MnN_y$ | Lattice parameter indexed with fcc or fct lattice | | | | | |
|---|---|---|---|---|---|---|---|---|---|
| | | | | Observed value | | | Reported value | | |
| | | | | a/nm | c/nm | c/a | a/nm | c/nm | c/a |
| $Mn_4N$ | 155 | 1.3–2.6 | – | 0.3865 | ---- | 1.000 | 0.3864[a] | ---- | 1.000[a] |
| $Mn_3N_2$ | 240 | 2.6–3.9 | – | 0.4206 | 1.3162 (0.4054*) | 2.832 (0.964**) | 0.4206[b] | 1.3132[b] (0.4044*) | 2.883[b] (0.961**) |
| $Mn_6N_{5\pm\delta}$ | 143 | 6.5 | 0.64 | 0.4199 | 0.4140 | 0.986 | | | |
| | 160 | 9.1 | 0.71 | 0.4221 | 0.4161 | 0.986 | 0.4221[c] | 0.4115[c] | 0.975[c] |
| | 174 | 25 | 1.07 | 0.4219 | 0.4151 | 0.984 | | | |
| | 186 | 25 | 1.08 | 0.4218 | 0.4155 | 0.985 | 0.4214[d] | 0.4148[d] | 0.984[d] |

a : $Mn_4N_{1.0}$ ($MnN_{0.25}$), b : $Mn_3N_{1.97}$ ($MnN_{0.66}$), c : $Mn_6N_{5.07}$ ($MnN_{0.85}$) and d : $Mn_6N_{5.52}$ ($MnN_{0.92}$).

The composition range of $Mn_6N_5$ phase was reported to be in a range between $MnN_{0.84}$ and $MnN_{0.95}$ at 573K in previous data [14]. *; the value of c/3a and **; the value of c/3.

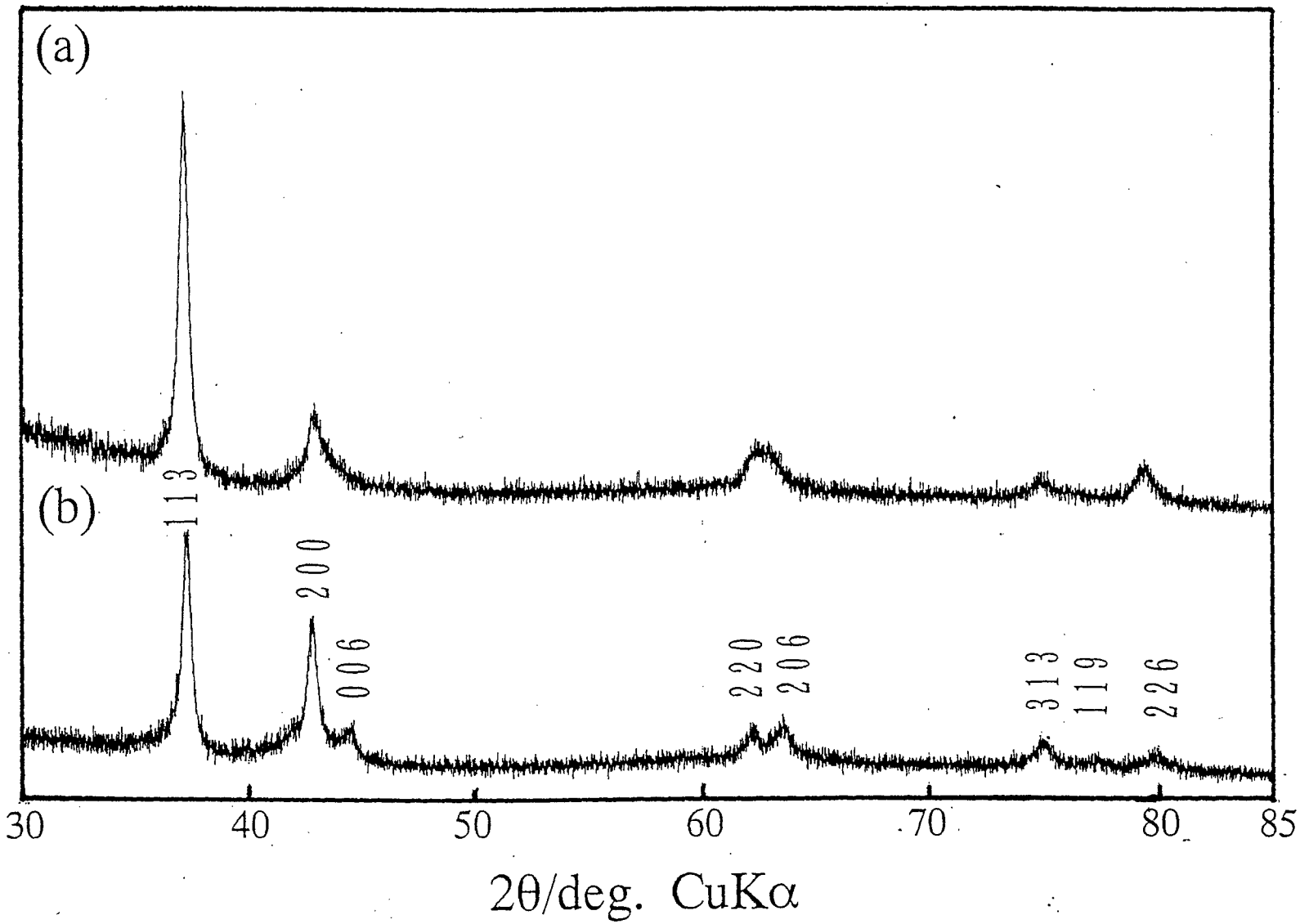


Fig. 5 X-ray diffraction patterns for the $MnN_{0.64}$ film deposited at $E_p$ of 143W and $p_N$ of 6.5Pa (a) and $Mn_3N_2$ powder deposited at $E_p$ of 240W and $p_N$ of 2.6Pa (b).

Fig. 6 depicts the variation of crystal phase as functions of $E_p$ and $p_N$. The $Mn_6N_{5\pm\delta}$ films were obtained over the relatively wide range of $E_p$ and $p_N$, especially in a larger $p_N$ region compared to $Mn_4N$ and $Mn_3N_2$. However, $Mn_3N_2$ became easy to deposit at the large $E_p$ region, even though $p_N$ was also large, because evaporation rate of Mn increased with a increase of $E_p$. While, in lower $p_N$ region, deposition of $Mn_3N_2$ preferred, but $Mn_4N$ was obtained only at low $E_p$ and $p_N$ region where the glow discharge was blinking.

### 3.2 *Electrical resistivity for the $MnN_y$ films*

Temperature dependence of the ratio of electrical resistivity to that at 295K, $\rho/\rho_{295}$, for the $MnN_y$ films is shown in Fig. 7. All of the $MnN_y$ films exhibited low resistivity in a range of 10–100μΩm at room temperature. These values for $MnN_y$ films are comparable to those of $Ni_3N$ powder (28μΩm at 273K) [12], but higher than those of TiN film (0.5–7μΩm) [9] and $Fe_4N$ sheet (1.62μΩm) [11]. It is seen in Fig. 7 that the temperature dependence of $\rho/\rho_{295}$ above 50K for $Mn_3N_2$ and $Mn_6N_{5+\delta}$ are metallic, but the $Mn_4N$ films exhibits semiconductive behavior. The metallic behavior of the $Mn_3N_2$ film is consistent with previous data for $Mn_3N_2$ [13]. The increase in $\rho/\rho_{295}$ of the $Mn_3N_2$ and $Mn_6N_{5+\delta}$ films with decreasing temperature below 50K may be related to the presence of the localized magnetic moments giving rise to the other scattering mechanism as Can't effect [15], because the magnetisms of $Mn_3N_2$ was reported to be antiferromagnetic [2]. $Mn_6N_5$ was presumed to be an antiferromagnetic compound [16]. The semiconductive behavior of $\rho/\rho_{295}$–$T$ curve of the $Mn_4N$ film may not reflect inherent property of $Mn_4N$ because of poor crystallinity. The value of $\rho/\rho_{295}$ of $Mn_6N_{5+\delta}$ films is found to keep almost constant close to 1 in the temperature region between 5 and 295K. Such a fact, i. e. small temperature dependence of ρ is similar to temperature dependence of ρ above superconducting transition temperature of some NaCl type compound with a lot of

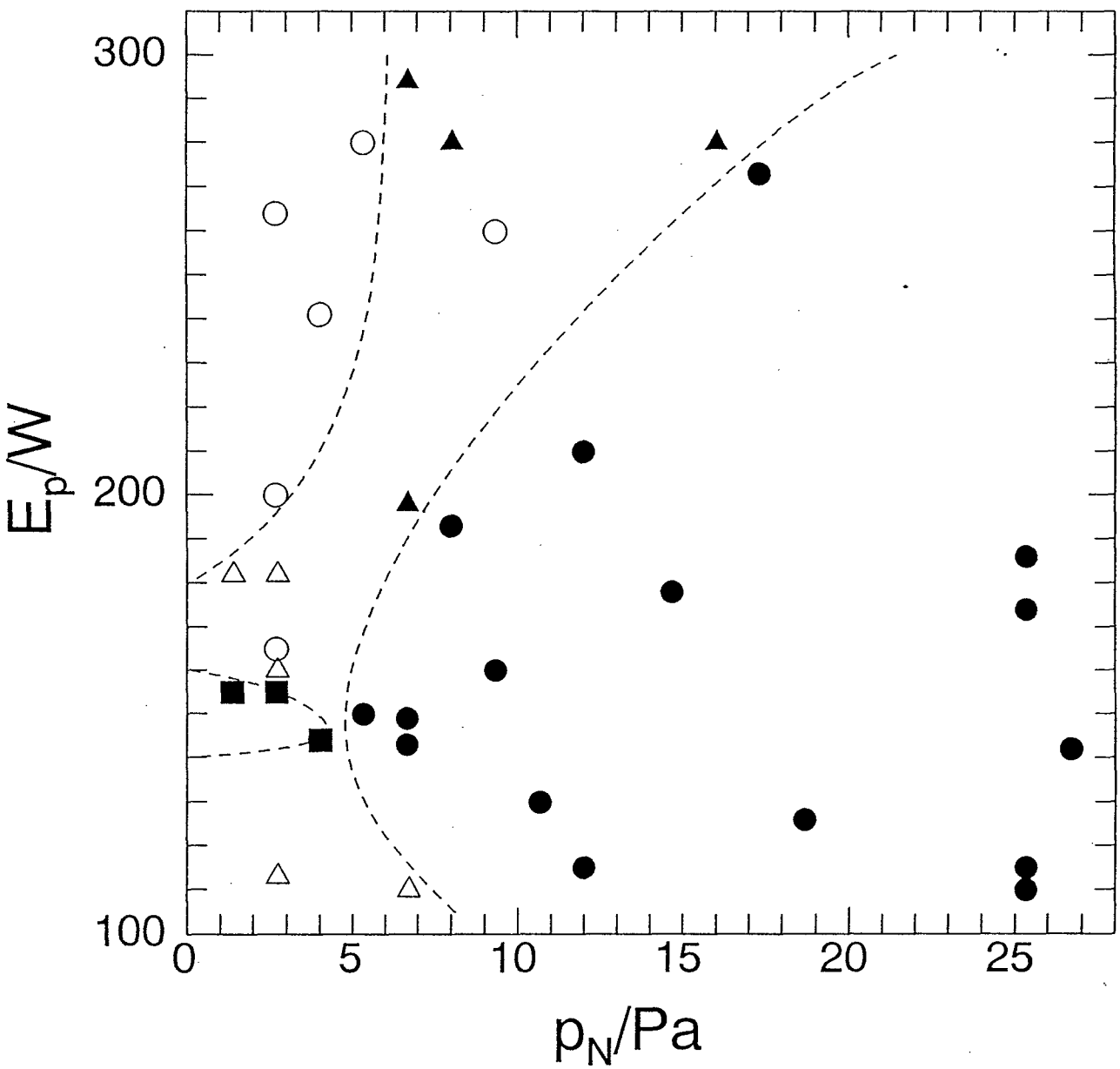


Fig. 6 The relation among crystal phase in products, nitrogen gas pressure during deposition ($p_N$) and electric power applied to W filament ($E_p$).

● : $Mn_6N_5$, ○ : $Mn_3N_2$, ■ : $Mn_4N$, ▲ : $Mn_6N_5$+$Mn_3N_2$, △ : $Mn_3N_2$ + $Mn_4N$.

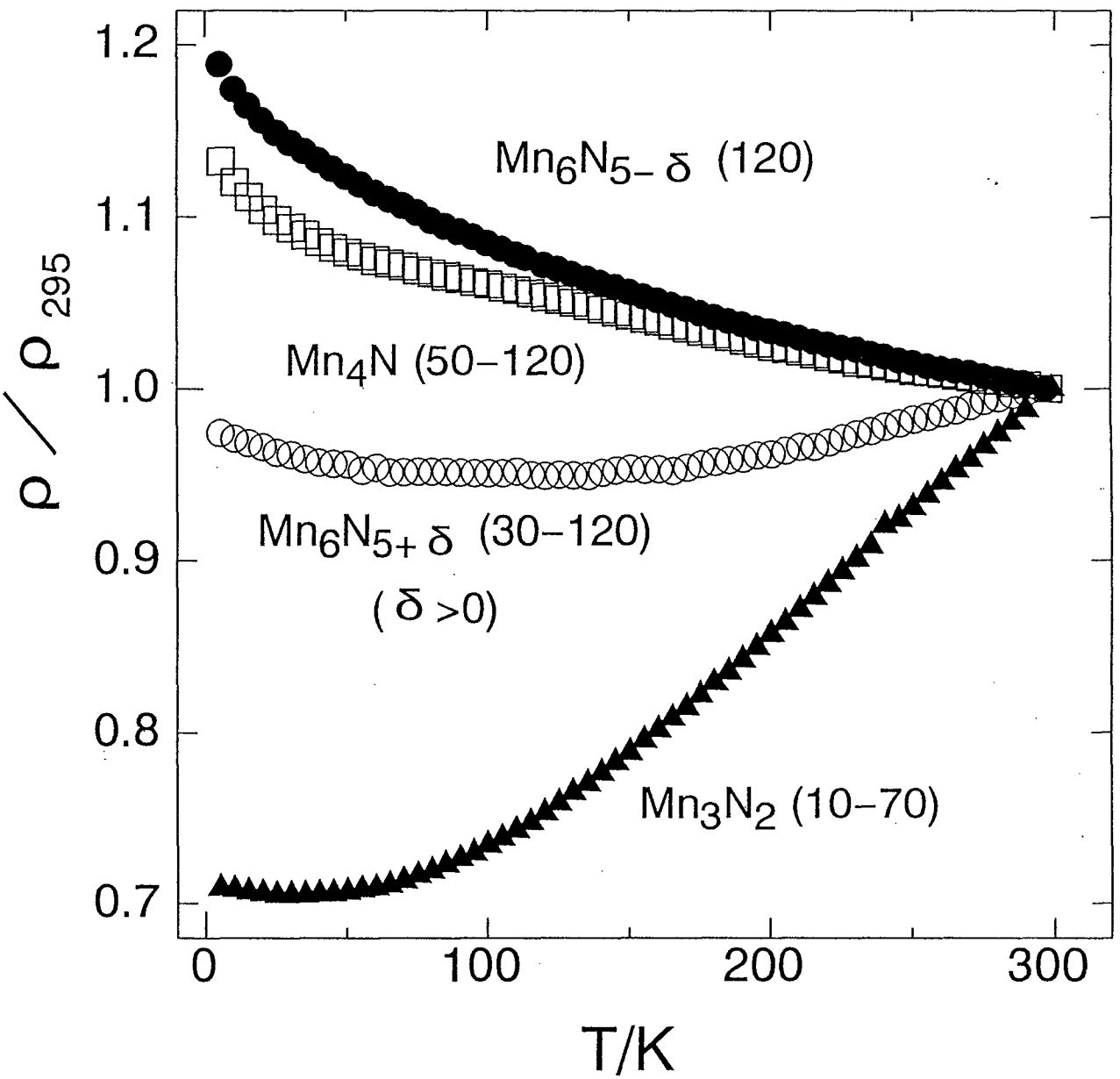


Fig. 7 Temperature dependence of electrical resistivity ratios ($\rho/\rho_{295}$) for $MnN_y$ films. $\rho_{295}$ denotes the electrical resistivity at 295K. The value of $\rho_{295}/\mu\Omega m$ for each samples is designated in parentheses.

vacancies such as TiO [17] and NbN [18]. The reason why TiO and NbN have little temperature dependence of ρ, is due to the large contribution of the electron scattering term by vacancies to ρ, because the term has little temperature dependence. While the $Mn_6N_{5-\delta}$ film exhibits a semiconductive behavior in temperature dependence of ρ, even though crystallinity, preferred orientation and thickness of the film are very similar to those of the $Mn_6N_{5+\delta}$ films. The $\rho/\rho_{295}$–$T$ curves of $Mn_6N_{5\pm\delta}$ films imply that they possess a lot of vacancies. There was a remarkable difference in sign of the temperature coefficient of ρ (TCR) between the $Mn_6N_{5+\delta}$ films and the $Mn_6N_{5-\delta}$ films. The semiconductive behavior of temperature dependence of $\rho/\rho_{295}$ for the $Mn_6N_{5-\delta}$ film may be attributed to the presence of too much number of N vacancies to exhibit metallic conductivity, because the vacancies scatter carriers. Such the difference in TCR between the $Mn_6N_{5\pm\delta}$ films is still unresolved. However, it have been reported that the sign of TCR of TiO or NbN is variable depending on their oxygen [17] or nitrogen content [18]. The differences in the signs of TCR of TiO with the different oxygen contents were attributed to a distinction in the electronic structures [17]. The difference in TCR between the $Mn_6N_{5\pm\delta}$ films may reflect that between their electric structures.

## 4. *Summary*

$Mn_4N$, $Mn_3N_2$ and $Mn_6N_5$ films were obtained by reactive vapor deposition method. The chemical composition of the films was controlled by regulating both of electric power applied to W filament and nitrogen gas pressure during the deposition. Deposited $Mn_6N_5$ films possessed the large nonstoichiometry of nitrogen. Temperature dependence of electrical resistivity for the $Mn_3N_2$ and the $Mn_6N_{5+\delta}$ films exhibit a metallic behavior. However, the $Mn_6N_{5-\delta}$ films exhibit a semiconducting behavior, even though the microstructure of $Mn_6N_{5-\delta}$ film is quite similar to that of $Mn_6N_{5+\delta}$ film. The slight dependence of $\rho/\rho_{295}$ of the $Mn_6N_{5+\delta}$ films may attributed to a lot of Mn and N vacancies.

*References*


1. F. Lihl, P. Ettmayer and A. Kutzelnigg, *Z. Metallkde.,* **53** (1962) 715.
2. G. Kreiner and H. Jacobs, *J. Alloys. Comp.,* **183** (1992) 345.
3. S. Nagakura and N. Ōtsuka, *J. Phys. Soc. Jpn.,* **39** (1975) 1047.
4. N. Ōtsuka, Y. Hanawa and S. Nagakura, *Phys. Status Solidi,* **A43** (1977) K127.
5. W. J. Takei, R. R. Heikes and G. Shirane, *Phys. Rev.,* **125** (1962) 1893.
6. M. Mekata, *J. Phys. Soc. Jpn.,* **17** (1962) 796.
7. M. Mekata, J. Haruna and H. Takaki, *J. Phys. Soc. Jpn.,* **25** (1968) 234.
8. M. Mekata H. Yoshimura and H. Takaki, *J. Phys. Soc. Jpn.,* **33** (1972) 62.
9. W. Tsai, M. Delfino, J. A. Fair and D. Hodul, *J. Appl. Phys.,* **73** (1993) 4462.
10. K. K. Shih, D. B. Dove and J. R. Crowe, *J. Vac. Sci. Technol.,* **A4** (1986) 564.
11. S. K. Chen, S. Jin, T. H. Tiefel, Y. F. Hsieh, E. M. Gyorgy and D. W. Johnson Jr., *J. Appl. Phys.,* **70** (1991) 6247.
12. R. Juza and A. Rabenau, *Z. Anorg. Allgem. Chem.,* **285** (1956) 212.
13. H. Jacobs and C. Stübe, *J. Less-Common Met.,* **96** (1984) 323.
14. N. A. Gokcen, *Bull. Alloy Phase Diagrams,* **11** (1990) 33.
15. J. Kondo, *Prog. Thor. Phys.,* **32** (1964) 37.
16. M. Tabuchi, M Takahashi and F. Kanamaru, *J. Alloys Comp., in press.*
17. S. Takeuchi and K. Suzuki, *Nippon Kinzoku Gakkaishi,* **33** (1969) 284.
18. L. E. Toth "Transition Metal Carbides and Nitrides" (Academic press, New York and London, 1971) p190.

## Chapter 6 Concluding Remarks

The magnetism of 3d metal nitrides $MN_y$ is generally similar to that of mother metals. On the other hand, the magnetic transition temperature of $MN_y$ varies greatly with their nitrogen content. In spite of the importance of the effect of nitrogen content on the magnetism, the relation between the number of nitrogen atom per a metal atom and the magnetism of $MN_y$ has been rarely studied except $FeN_y$. Furthermore, the magnetic properties of $MN_y$ with the same crystal structure were affected considerably by a kind of metal. In order to clarify the effect of nitrogen content on the magnetism of 3d metal nitrides, the relationships between nitrogen content and the magnetic property and also the relationship between the number of valence electrons and magnetism are necessary to examined systematically.

Metal atoms in 3d metal nitrides often distribute at different lattice sites which take different N–coordination number each other. In such a case, magnetic moment per a metal atoms in a nitride varies with the N–coordination number of metal atom ($z_N$), i.e. the metal atom with larger N–coordination number possesses smaller magnetic moment. The mechanism of such the different magnetic moments of atom by atom in $MN_y$ was explained on $Fe_4N$ as follows [1, 2]. The crystal structure of $Fe_4N$ is shown in Fig. 1 (a) in chapter 1. It can be visualized as an fcc sublattice of Fe with an additional N atom at the center of the cell. There are two kinds of Fe atoms occupy different lattice sites each other, i.e., (i) the Fe atoms at the cube corner positions (hereafter referred to as Fe(1)) and (ii) the Fe atoms at the face center positions (hereafter referred to as Fe(2)). The crystallographic position of N results in shorter Fe(2)–N distances than Fe(1)–N ones ($d$(Fe(2)–N) ≈0.190nm; $d$(Fe(1)–N) ≈0.329nm). These geometrical considerations suggest that the Fe–N interactions would preferentially occur between face–centered Fe and central N atoms rather than between corner Fe and N atoms. The magnetism of $Fe_4N$ was ferromagnetic with $T_c$ of 761K [3] and different values of magnetic moment for Fe(1) and

Fe(2) atoms was observed [4] ($\mu_{Fe(1)}=3\mu_B$; $\mu_{Fe(2)}=2\mu_B$). The occurrence of larger $\mu_{Fe}$ is explained by a band theory appeared at Appendix in chapter 2 [1, 2]. Consequently, the distribution of $\mu_M$ have to be taken into account for the consideration of the magnetic property. The effect of nitrogen content on the magnetism was examined in the Mn–N system, because manganese nitrides $MnN_y$ possess various crystal phases over a wide range of $y$ ($0<y<1$). The shortest Mn–Mn distance in $MnN_y$ increases linearly with increasing their nitrogen content. The interatomic distance $r_{M-M}$ between paramagnetic atoms generally correlate to not only exchange coupling constant $|J_{M-M}|$ and but also magnetic moment per a M atom ($\mu_M$). A strong correlation between $T_{mag}$ and $r_{M-M}$ was observed in $MnN_y$ and Mn alloys, both of which have fcc and fct Mn–sublattice. However, the $T_{mag}$–$r_{M-M}$ plot of $Mn_{2-3}N$ and $Mn_2N$, which have hcp Mn sublattice, deviated from a tendency in the $T_{mag}$–$r_{M-M}$ plot of fcc or fct $MnN_y$ and Mn alloys. Therefore the correlation between $\mu_M$ and $T_{mag}$ was examined. The magnetic moment of the Mn atom at the lattice site in $MnN_y$ is strongly affected by numbers of nitrogen adjacent the Mn atom above described on $Fe_4N$. As seen in the result of neutron diffraction of $Mn_3N_2$, the largest $\mu_M$ in $MnN_y$ generate on the Mn atom with the smallest $z_N$ in any cases. The following magnetic moment of Mn atom were used for each N–coordination number $z_N$; $2.4\mu_B$ for $z_N=0$, $0.9\mu_B$ for $z_N=2$, $1.6\mu_B$ for $z_N=3$, $3.4\mu_B$ for $z_N=5$. In this work, a linear relationship between $T_{mag}$ and the largest $\mu_M$ in $MnN_y$ with $0\leqq y<1$ is first discovered. Through the investigation of the effect of nitrogen on the magnetic properties of $MnN_y$ ($0\leqq y<1$), the $\mu_{Mn}$ of the Mn atom with smaller N–coordination number were found to relate to $T_{mag}$. Such a linear relationship between the largest $\mu_M$ and $T_{mag}$ was also observed for $FeN_y$ ($0\leqq y<0.5$) with the nearly closest–packed structure such as of Fe atoms. These findings indicate that $T_{mag}$ of $MN_y$ with nearly closest–packed structure of 3d metals correlate closely to the largest $\mu_M$ in $MN_y$, which is its magnetic moment of the M atom with smallest N–coordination number. Consequently, it may be concluded

that the magnitude of largest $\mu_M$ is important parameter rather than $r_{M-M}$ correlated to "magnetovolume effect" to explain the effect of nitrogen on the magnetic transition temperature of $MN_y$.

In the system of $M_2N$ (M=Mn, Fe, Co), the effective magnetic moments were observed to be varied with the number of valence electrons of the M atom. In the system of $M_{2-3}N$, (M=Fe, Co, Ni), the effective magnetic moments decreased monotonously with increasing the number of valence electrons of the M atom. These relations between the effective moments and the number of valence electrons per a M atom for $M_2N$ and $M_3N$ are similar to those for 3d metals and their borides and phosphides, in which the effective magnetic moments or the magnetic moments varies with the number of valence electrons in such a way "Slater–Pauling curves".

The values of effective magnetic moments for $Co_3N$, $Co_2N$ and $Ni_3N$ are determined to be 1.4±0.1, 0.65±0.05 and 0.48±0.04$\mu_B$, respectively. The difference in the effective magnetic moments between $Co_3N$ and $Co_2N$ may be related to the difference in N–coordination numbers around the Co atom between them, i.e. $\mu_{eff}$ of $Co_3N$ with the N–coordination number of 2 is larger than that of $Co_2N$ with the N–coordination number of 3. This result is consistent with the tendency observed at $MnN_y$ and $FeN_y$.

$Mn_4N$, $Mn_3N_2$ and $Mn_6N_5$ films free from oxides which hampers characterization of $MnN_y$ were prepared successfully by reactive vapor deposition method, and their electric resistivity were measured. The chemical composition of the films was controlled by regulating both of electric power applied to W filament and nitrogen gas pressure during the deposition. Deposited $Mn_6N_5$ films possessed the large nonstoichiometry of nitrogen. Temperature dependence of electrical resistivity for the $Mn_3N_2$ and the $Mn_6N_{5+\delta}$ films exhibit a metallic behavior. However, the $Mn_6N_{5-\delta}$ films exhibit a semiconducting behavior, even though the microstructure of $Mn_6N_{5-\delta}$ film is quite similar to that of $Mn_6N_{5+\delta}$ film. The slight dependence of $\rho/\rho_{295}$ of the $Mn_6N_{5+\delta}$ films may be attributed

to a lot of Mn and N vacancies.

It is found as the effect of nitrogen content on the magnetic transition temperature that the magnitude of the largest magnetic moment of the M atom with smallest N–coordination number correlates closely with the magnetic transition temperature of $MN_y$ with nearly closed–packed arrangement of M atoms.

*References*

1 J. Kanamori, *Prog. Theor. Phys. Suppl., 101* (1990) 1.

2 A. Sakuma, *Nippon Oyo Jiki Gakkaishi, 17* (1993) 741.

3 G. W. Wiener and J. A. Berger, *J. Met., 7* (1955) 360.

4 B. C. Frazer, *Phys. Rev., 112* (1958) 751.

**Paper relevant to this study**

M. Tabuchi, M. Takahashi and F. Kanamaru, "Relation between magnetic transition temperature and magnetic moment for manganese nitrides $MnN_y$ ($0<y<1$)" *J. Alloys. Comp.,* in press.

**Acknowledgments**

The author would like to express his greatest gratitude to Professor F. Kanamaru of Osaka University for his continuing guidance, helpful discussion and support in coordinating this work. He would also like to acknowledge the valuable discussion technical guidance for experiment and kind advice of Dr. M. Takahashi of Osaka University during this investigation. He also wishes to express his heartfelt thanks to Drs. S. Kikkawa and K. Nobugai of Osaka university for the helpful advice. The kind guidance and critical reading of this thesis of Profs. S. Kawai and M. Sorai of Osaka University are also gratefully acknowledged. He sincerely acknowledges to Mr. K. Tanihata of ISIR in Osaka University for DTA–TG measurement. He would like to thank Dr. M. Kakeshita of Osaka University for his suggestions and guidance. Acknowledgment are also due to Drs. T. Yamamoto of Central Research Institute of Electric Power Industry, N. Cho of Korea Institute of Science and Technology, and G. Er and all members of Kanamaru Laboratory for their kind advice and encouragement.

He wishes to thank Dr. K. Ado of Government Industrial Research Institute, Osaka for his kindness offer us to his Faraday balance and Dr. I. Matsubara of Government Industrial Research Institute, Osaka for determination of nitrogen and oxygen in samples. Acknowledgement is due to Ms., F. Fukuda of MAC in ISIR, Osaka university, for CHN analysis. The authors also wishes to thank Messrs. A. Omura, H. Yamaguchi, H. Matsukawa, N. Ogawa, M. Kakuichi and M. Ōnishi of Workshop in ISIR, Osaka university, for making the apparatus for the reactive vapor deposition.